Lithos 396–397 (2021) 106238

Contents lists available at ScienceDirect

Lithos

journal homepage: www.elsevier.com/locate/lithos

Research Article

Iron isotope and trace metal variations during mantle metasomatism: In situ study on sulfide minerals from peridotite xenoliths from Nógrád-Gömör Volcanic Field (Northern Pannonian Basin)

Levente Patkó [a,b,c], Jakub Ciazela [d,*], László Előd Aradi [a], Nóra Liptai [b], Bartosz Pieterek [e], Márta Berkesi [a,b], Marina Lazarov [f], István János Kovács [b], François Holtz [f], Csaba Szabó [a]

[a] Lithosphere Fluid Research Lab (LRG), Eötvös Loránd University, Budapest, Hungary
[b] Lendület Pannon LitH$_2$Oscope Research Group, EK, Budapest, Hungary
[c] Geodetic and Geophysical Institute, Research Centre for Astronomy and Earth Sciences (CSFK), Sopron, Hungary
[d] Institute of Geological Sciences, Polish Academy of Sciences, Warsaw, Poland
[e] Institute of Geology, Adam Mickiewicz University, Poznań, Poland
[f] Institut für Mineralogie, Leibniz Universität Hannover, Hannover, Germany

ARTICLE INFO

Article history:
Received 1 January 2021
Received in revised form 13 May 2021
Accepted 13 May 2021
Available online 18 May 2021

Keywords:
Mantle xenoliths
Wehrlitic metasomatism
Sulfide and chalcophile element enrichment
Fe isotope

ABSTRACT

Sulfides from lherzolite and wehrlite xenoliths from the Nógrád-Gömör Volcanic Field (NGVF), located in the Northern Pannonian Basin, were studied to understand the behavior of chalcophile and siderophile elements during mafic melt – peridotite interaction. We applied in situ methods to analyze the major and trace elements, as well as Fe isotope compositions of sulfide minerals. Sulfides are more abundant in wehrlites (~0.03 vol%) and are often enclosed in silicates, whereas in lherzolites, they are scarcer (~0.01 vol%) and predominantly interstitial. Monosulfide solid solution and pentlandite are the most common sulfide phases in the lherzolite xenoliths, whereas in wehrlite xenoliths it is pyrrhotite and chalcopyrite. Consequently, wehrlitic sulfides show higher bulk Fe and Cu but lower bulk Ni and Co contents compared to the lherzolitic sulfides. Trace elements with both chalcophile and siderophile character (Ge, Se, Te, and Re) show lower, whereas highly chalcophile elements (Zn, Cd, Sb, and Tl) show higher concentrations in wehrlitic sulfides compared to lherzolitic ones. Highly siderophile elements show no systematic difference between the sulfides of the two xenolith series, which suggests moderate enrichment in these elements in wehrlite bulk rocks due to their higher sulfide content. Sulfide δ^{56}Fe signature indicates variable isotopic composition both in lherzolites (δ^{56}Fe: −0.13 to +0.56‰) and wehrlites (δ^{56}Fe: −0.20 to +0.84‰) relative to the terrestrial mantle (δ^{56}Fe: +0.025 ± 0.025‰; Craddock et al., 2013). However, irrespectively of the xenolith lithology, there is a significant difference between the δ^{56}Fe of sulfides from the two sampling localities: NTB /North/: vary from −0.20 to +0.04‰ and NME /South/: vary from +0.56 to +0.84‰. This suggests that the Fe isotopic ratios of sulfides are not modified by the wehrlitization process. Difference in sulfide δ^{56}Fe between the two xenolith localities is probably because of the higher, isotopically heavier (δ^{56}Fe: from +1.28 to +1.60‰; Ciążela et al., 2019) chalcopyrite content in sulfides from the NME xenoliths compared to those from the NTB xenoliths irrespectively to their lithology. Our results also indicate sulfide and chalcophile element enrichment resulting from metasomatism in the subcontinental lithospheric mantle. We suggest that this process affected the regional metal distribution and has implications for global metal mass balance within the subcontinental lithosphere.

1. Introduction

Sulfides are the main hosts of elements with chalcophile (Zn, Bi, Cu, Ag, Cd, Pb, Tl, Re, Ge, Se, Te, As, Sb) and siderophile (Os, Ir, Ru, Rh, Pt, Pd, Au, Re, Ge, Se, Te, As, Sb) characteristics (e.g. Lorand and Luguet, 2016). Therefore, studying sulfides in peridotites is essential to understand the budget of these elements in the upper mantle. In silicate-sulfide systems, sulfides start melting at relatively low temperature (<1100 °C at 1 GPa; Zhang and Hirschmann, 2016), and thus may be involved in partial melting and subsequent melt migration. Indeed, both depleted (e.g. Luguet et al., 2007; Szabó and Bodnar, 1995) and metasomatically modified (e.g. Aulbach et al., 2021; Wainwright et al., 2015) sulfides were observed in natural mantle samples from various tectonic settings. Sulfides also occur frequently in pyroxenites, representing immiscible sulfide melts (e.g. Aulbach et al., 2009). Although the average sulfide

* Corresponding author.
E-mail address: j.ciazela@twarda.pan.pl (J. Ciazela).

https://doi.org/10.1016/j.lithos.2021.106238

abundance in the Earth's mantle is only ~0.07 vol% (Fellows and Canil, 2012), sulfides can influence physical properties of the mantle, resulting in increased density (Mungall and Su, 2005), electrical conductivity (Ducea and Park, 2000) and lowered peridotite solidus (Zhang and Hirschmann, 2016).

Studies on mantle sulfides have generally been focusing on the characteristics of platinum group elements (PGE) and *Re*—Os isotope systematics (Luguet and Reisberg, 2016 and references therein; González-Jiménez et al., 2020), mostly based on bulk rock analyses. However, it is evident that in situ analyses can reveal more details on the complexity of the sulfide characteristics (e.g. Griffin et al., 2002). In the last two decades, an increasing amount of in situ data from mantle sulfides was published (Alard et al., 2000, 2011; Aulbach et al., 2019, 2021; Ciążela et al., 2018; Delpech et al., 2012; D'Errico et al., 2019; González-Jiménez et al., 2014; Guo et al., 1999; Saunders et al., 2015, 2016; Wang et al., 2018).

In this paper, we present detailed analyses on major and trace element, as well as Fe isotopic compositions of enclosed and interstitial sulfides from upper mantle lherzolite and wehrlite xenoliths, collected in volcanic rocks from the northern part of the Pannonian Basin. To understand the behavior of siderophile and chalcophile elements during wehrlitization, we performed detailed in situ petrographic, major and trace element, and Fe isotope analyses of the sulfides. As observed by Ciążela et al. (2017, 2018) in oceanic settings, especially along the crust-mantle transition zone and uppermost mantle, the elevated modal proportion of sulfides may indicate that upward migrating primitive melts lose a significant portion of their metal load beneath the crust due to melt-peridotite interactions. Our results indicate that this observation can be extended to the subcontinental mantle, suggesting that subcrustal metal enrichment along melt migration channels is a common and potentially even a global phenomenon.

2. Geological background and summary of NGVF ultramafic xenoliths

The Pannonian Basin in Central Europe is framed by the Alpine, Carpathian and Dinaric orogenic belts (Fig. 1a). The basin started to form with the juxtaposition of two tectonic mega-units, ALCAPA and Tisza-Dacia, in the late Oligocene (e.g. Fodor et al., 1999). Significant extension, driven by the subduction rollback on the eastern margin of the region, took place during the Neogene (e.g. Horváth et al., 2006). Considerable thinning of the lithosphere and resulting asthenospheric doming occurred in the Pannonian Basin during the extensional period (Horváth, 1993). Finally, the collision of the mega-units (ALCAPA and Tisza-Dacia) with the stable European platform gradually transformed into a compressive tectonic regime from the late Miocene (Horváth and Cloetingh, 1996).

All stages of the basin evolution were accompanied by widespread volcanism including silicic, calc-alkaline, and alkali products (e.g. Szabó et al., 1992). The formation of monogenetic alkali basalts, such as at the ones comprising the study area of Nógrád-Gömör Volcanic Field (NGVF) (Fig. 1b), can be explained by adiabatic decompression melting of the asthenosphere related to upwelling which is associated with the extension (~20–8 Ma) (e.g. Embey-Isztin et al., 1993). The volcanic activity in the NGVF took place between 7.0 and 0.3 Ma based on combined U/Pb and (U—Th)/He geochronometry (Hurai et al., 2013).

The alkali basalts in the NGVF host a great number of ultramafic xenoliths, which have been the focus of numerous studies in the past decades. Therefore, a robust database is available for geochemical compositions (e.g. Liptai et al., 2017; Patkó et al., 2020; Szabó and Taylor, 1994), physical properties (e.g. Liptai et al., 2019) and fluid and melt compositions (e.g. Zajacz et al., 2007) of these xenoliths. Yet, so far only two works (Szabó and Bodnar, 1995; Zajacz and Cs, 2003) have been dedicated to the chemical characterization of sulfides hosted by the xenoliths. Szabó and Bodnar (1995) distinguished sulfides trapped during metasomatic and partial melting events. They

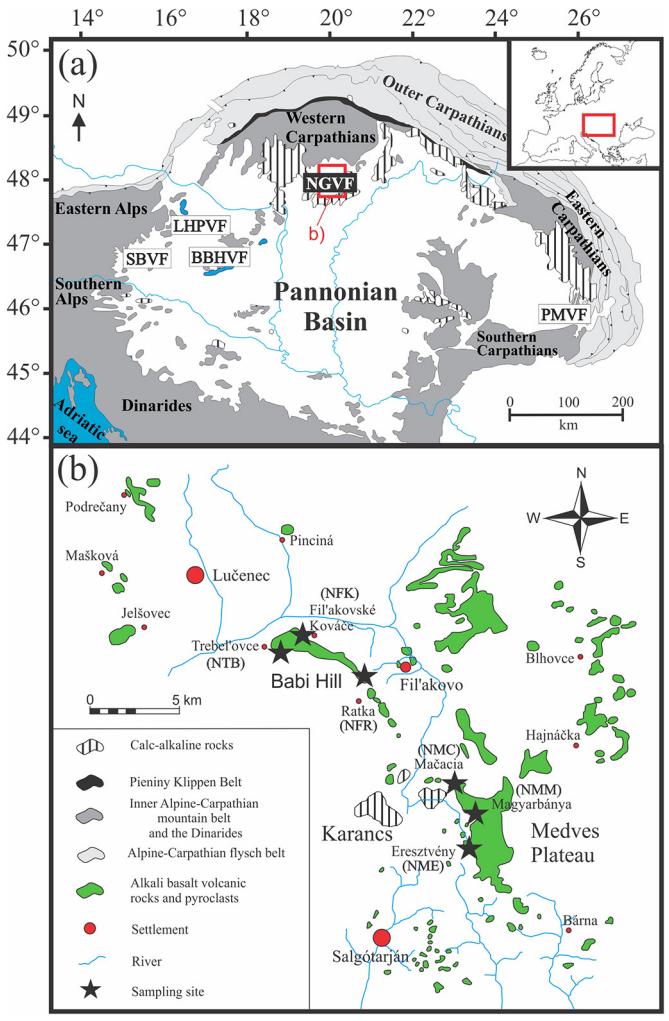

Fig. 1. (a) Simplified geological map of the Carpathian-Pannonian region. The xenolith-bearing Neogene alkali basalt occurrences are marked using abbreviations: SBVF, Styrian Basin Volcanic Field; LHPVF, Little Hungarian Plain Volcanic Field; BBHVF, Bakony–Balaton Highland Volcanic Field; NGVF, Nógrád-Gömör Volcanic Field; PMVF, Perşani Mountains Volcanic Field. **(b)** Alkali basalt occurrences and upper mantle xenolith sampling locations in NGVF including Trebel'ovce (NTB), Fil'akovské Kováče (NFK), Ratka (NFR), Mačacia (NMC), Magyarbánya (NMM) and Eresztvény (NME). Geological maps are modified after Patkó et al. (2020) and references therein.

also revealed sulfide prevalence and geochemical difference between partial melting derived sulfides in xenoliths with equigranular and recrystallized textures versus sulfides in xenoliths with protogranular/porphyroclastic textures, meaning higher modal abundance and Ni (+Co) - Cu enrichment in the former xenoliths. Therefore, they concluded that recent deformation and recrystallization, also supported by Liptai et al. (2019), has significantly affected the sulfides. The sulfides in cumulate xenoliths studied by Zajacz and Cs (2003) are enriched in Fe and likely precipitated from a sulfide melt coexisting with a silicate melt.

The ultramafic xenoliths hosted by the NGVF basalts can be divided into lherzolite, wehrlite and cumulate series. Wehrlite xenoliths are products of mantle metasomatism that took place between the peridotite wall rock and a mafic silicate melt (Patkó et al., 2020), whereas the dominantly pyroxenite cumulates are crystallized products from basaltic melts emplaced on the boundary of the lithospheric mantle and lower crust (Kovács et al., 2004). The wehrlites and cumulates are petrographically and geochemically rather uniform; in contrast, the lherzolites can be classified into four subgroups with different evolution (Liptai et al., 2017). The Group IA lherzolites show depleted character

with a high olivine Mg# (Mg/[Mg + Fe_{tot}]) of ≥89 and low rare earth element (REE) concentrations (ΣREE <25 ppm) in clinopyroxenes, likely representing partial melting residues (Liptai et al., 2017). The Group IIA lherzolites, which occur only in the northern part of the NGVF, contain Nb-poor amphiboles, and presumably formed by a subduction-related volatile-rich silicate melt. The formation of Groups IB and IIB are linked to two different metasomatic events. Metasomatism of Group IB xenoliths is characterized by U-Th-Nb-Ta- and light rare earth element (LREE)-enrichment in amphibole and clinopyroxene, whereas Group IIB xenoliths are enriched in Fe, Mn, Ti, and LREE in all rock forming minerals (Liptai et al., 2017). In this study, we examined xenoliths of the aforementioned non-cumulate wehrlite and three (Group IA, IB, IIB) lherzolite groups.

3. Sampling localities and studied materials

Over 80 lava-hosted xenoliths were studied from quarries in the central part of the volcanic field, which are from north to south: Trebel'ovce [NTB], Fil'akovské Kováče [NFK], Ratka [NFR], Mačacia [NMC], Magyarbánya [NMM] and Eresztvény [NME] (Fig. 1b; Supplementary Table 1). Based on the petrographic features (abundance, size, and fresh appearance) of sulfide grains, we selected a representative set of 8 lherzolite and 11 wehrlite xenoliths to analyze the major element composition of sulfide minerals. Among the 8 lherzolite xenoliths, two belong to Group IA (NTB0307, NME1116), one to Group IB (NFR0309) and five to Group IIB (NTB1122, NFK1115, NFR1109, NMC1309, NMM0318) according to the classification of Liptai et al. (2017). The wehrlites include weakly (NTB1109, NFR1119B, NMC1302B; olivine Mg# > 0.87; clinopyroxene Mg# > 0.88 and spinel Cr# > 0.19), moderately (NFK1137A, NMM1114, NME1110, NME1129D) and strongly metasomatized (NTB1120, NFK1110, NFR1117A, NMM1129; olivine Mg# < 0.86; clinopyroxene Mg# < 0.86 and spinel Cr# < 0.20) xenoliths (Patkó et al., 2020). The weakly and strongly metasomatized wehrlite xenoliths were formed under low (<0.3) and high (>0.3) melt/rock ratio, respectively (Patkó et al., 2020). Trace elements and Fe stable isotopes in sulfide minerals were analyzed in 2 lherzolites (NTB1122, NME1116) and 4 wehrlites (NTB1109, NTB1120, NME1110, NME1129D), all from the Trebel'ovce (NTB) and Eresztvény (NME) localities (Fig. 1b). Rock-forming minerals of the Trebel'ovce and Eresztvény wehrlite xenoliths display the largest variability in major (e.g. Fe, Mn, Ti) and trace element (e.g. Nb, Ta, Hf, Zr) concentrations, which is related to the wehrlitization (Patkó et al., 2020).

4. Analytical techniques

4.1. Polarized light and scanning electron microscopy (SEM)

The petrography of the xenoliths was studied with a Nikon Eclipse LV100 POL polarizing microscope at the Lithosphere Fluid Research Laboratory (LRG) and an AMRAY 1830 I/T6 scanning electron microscope at the Department of Petrology and Geochemistry, Faculty of Science of the Eötvös Loránd University (Budapest). The modal composition of the sulfides was determined using Corel PhotoPaint X8 program of the Corel X8 software package based on the area of the different sulfide phases.

4.2. Electron microprobe analyses (EMPA)

The major element composition of the sulfide phases (monosulfide solid solution-mss, pentlandite, pyrrhotite, chalcopyrite) were determined using CAMECA SX-50 and CAMECA SX-100 electron microprobes at the CNR Institute for Geosciences and Earth Resources (IGG), Padua, Italy and at the Institute of Mineralogy, Leibniz University of Hannover, Germany, respectively. The operating conditions were 20 kV accelerating voltage and 20 nA beam current in Padua, and 15 kV accelerating voltage and 15 nA beam current in Hannover. Counting times were 10 s at the peak and 5 s at the background for major elements in both laboratories. The X-ray counts were converted into oxide weight percentages using the PAP correction program (Pouchou and Pichoir, 1991). Calibration was carried out based on the following standards in both laboratories: native metals (Cu, Co), pyrite (S, Fe), and synthetic Ni-oxide (Ni).

4.3. Laser Ablation Inductively Coupled Plasma Mass Spectrometry (LA-ICP-MS)

4.3.1. Trace element analyses

Trace element concentrations of the sulfides were obtained at the Institute of Mineralogy, Leibniz University of Hannover, Germany, using an ELEMENT-XR (Thermo Scientific, Germany) fast-scanning sector field ICP-MS coupled to a femtosecond laser ablation (fs-LA) system (Solstice, Spectra-Physics, USA). The wavelength of the laser was 194 nm and the yielded energy pulses at samples were < 50 μJ in the fourth harmonic. The advantage of the ultra violet laser beam with the ultrashort pulses is the prevention of elemental fractionation and minimization of matrix effects. In fs-LA-ICP-MS systems, the energy density is only 1.5 J/cm^2 (e.g. Horn and von Blanckenburg, 2007). The femtosecond pulses deposit the energy faster onto the target material than thermal diffusion transports the energy away from the ablation area. This allows ablated materials to be immediately heated to supercritical temperatures. Horn and von Blanckenburg (2007) estimated elemental fractionation to be smaller than the internal precision achievable during fs-LA-ICP-MS analyzes (0.4%, 2SD). Repetition rates of 10 Hz and 10–28 Hz, and spot sizes of 60 μm and 30–60 μm were used for standards and sulfide grains, respectively. The carrier gas was He mixed with Ar immediately after its exit from the ablation cell and prior to entrance in the ICP-MS. Oxide formation was below 0.4% based on the ThO/Th ratio during ICP-MS tuning.

For covering all elements of interest, both NIST-610 and PGE-A reference materials were used as external standards. For internal standards, we used the average Ni concentrations, which were previously measured with EMPA. Data reduction and drift correction was carried out with the Matlab-based SILLS (Signal Integration for Laboratory Laser System) software (Guillong et al., 2008). Although the accuracy is difficult to ascertain for all the elements, it can be estimated based on the few elements occurring in both the measured standards (i.e. NIST 610 and PGE-A). For example, our accuracy for Se is ~31 % (163 ± 15 ppm (1 SD, n = 22) measured in PGE-A in reference to NIST-610 vs. 236 ppm obtained by Lorand and Alard (2001) and our accuracy for Au is ~16 % (234 ± 23 ppm (1 SD, n= 22) measured in PGE-A in reference to NIST-610 vs. 274 ppm obtained by Lorand and Alard (2001).

The degree of potential contamination with silicates was controlled by measurement of Si, which barely (<10% of all analyzes) reached 5 wt%. The light PGE (^{99}Ru, ^{101}Ru, ^{103}Rh, ^{105}Pd, and ^{106}Pd) isotopes required interference correction for the argides of ^{66}Zn, ^{63}Cu, ^{65}Cu, ^{61}Ni, and ^{59}Co isotopes. The correction of the interferences was done by measuring the ZnS (Mineralogical Association of Canada (MAC)), native Ni, native Cu, and Co-rich pyrite (MAC) reference materials for comparison of the pure metal signals with the metal argide signals. The corrected results only slightly differ from the measured raw data (<15% for Ru, <10% for Rh and < 5% for Pd). Given that the rates of argide formations were determined with imprecisions of 9% for Ru, 8% for Rh and 10% for Pd, the uncertainties caused by applied corrections are 0.06% for Ru, 0.08% for Rh, and 0.5% for Pd.

We analyzed non-altered sulfides in order to avoid geochemical bias due to late stage alteration (e.g. oxidation). We carried out analyzes on bulk sulfides, except sulfide grain 7a in NTB1122/section 2 (Supplementary Table 5). Therefore, the distribution of trace elements among low-temperature phases do not affect our data. Since the rock-forming silicates contain extremely low concentrations of chalcophile and siderophile trace elements, the effect of ablation of small silicate volumes on the concentration of the measured elements is negligible or minor.

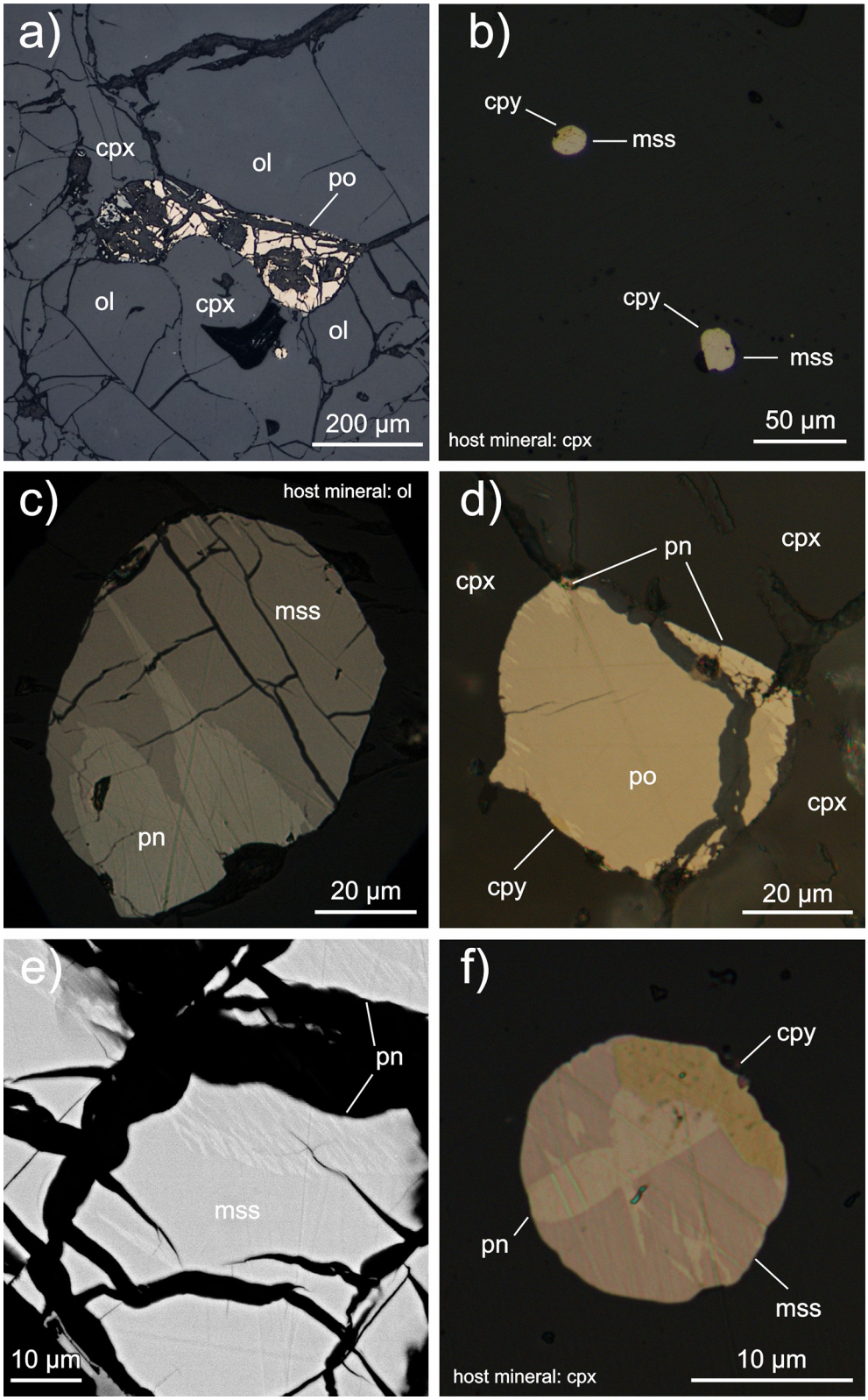

Fig. 2. Sulfides with different mineral composition and textural positions from the Nógrád-Gömör lherzolite and wehrlite xenoliths. **(a)** Partially oxidized interstitial sulfide (no. 9) between silicate grains in the NME1129D wehrlite xenolith (reflected light image). **(b)** Enclosed sulfides (no. 18 and 19) hosted in clinopyroxene from the NFK1137A wehrlite xenolith (reflected light image). **(c)** Typical lherzolitic sulfide (no. 2) composed of mss and pentlandite in the NFR1109 lherzolite xenolith (reflected light image). **(d)** Typical wehrlitic sulfide (no. 1f) with prevailing pyrrhotite in the NTB1120 wehrlite xenolith (reflected light image). **(e)** Pentlandite exsolutions (bright) in mss (dark) (grain no. 2) in the NTB0307 lherzolite xenolith (back-scattered SEM image). **(f)** Massive chalcopyrite (cpy) at the edge of the sulfide (no. 7a) in the NMM0318 lherzolite xenolith (reflected light image). Abbreviations: mss - monosulfide solid solution; pn - pentlandite; po - pyrrhotite; cpy - chalcopyrite; ol - olivine, cpx - clinopyroxene.

4.3.2. Iron isotope analyses

In situ iron isotopes of sulfides were determined using the aforementioned fs-LA system combined with a NeptunePlus (Thermo Scientific, Germany) multi-collector ICP-MS operating in high resolution mode at the Institute of Mineralogy, Leibniz University of Hannover, Germany. Detailed instrumental and measurement settings were as described by Horn and von Blanckenburg (2007) and Oeser et al. (2014). The only difference compared to the method of these studies is that we used standard-sample bracketing for the instrumental mass bias correction in our study. We report our results as δ^{56}Fe and δ^{57}Fe (i.e., deviations of $^{56}Fe/^{54}Fe$ and $^{57}Fe/^{54}Fe$ in ‰ relative to IRMM-014 standard) based on the following equations (Oeser et al., 2014):

$$\delta^{56}Fe = \left[\left(\frac{(^{56}Fe/^{54}Fe)_{sample}}{(^{56}Fe/^{54}Fe)_{reference}}\right)-1\right]x1000 \quad \delta^{57}Fe = \left[\left(\frac{(^{57}Fe/^{54}Fe)_{sample}}{(^{57}Fe/^{54}Fe)_{reference}}\right)-1\right]x1000$$

During every analytical session, an in-house JM puratronic (PURA) Fe-standard (99.995% Puratronic, Johnson Matthey, lot No. FE495007IF2) was repeatedly measured (Supplementary Table 6) to make sure that the operating conditions were optimal. All samples and the PURA standard were analyzed with a repetition rate of 3 Hz, whereas it was 11 Hz for the IRMM-014 standard measurements. We used a laser beam with a diameter of 20–40 μm for sulfides and 60 μm for standards (Supplementary Table 6). Only results that follow terrestrial fractionation line of δ^{56}Fe and δ^{57}Fe were reported. The size of the sulfide grains (dominantly <40 μm in diameter) requires spot rather than raster analysis, which limits the measurement time to 30–40 s, lowers the counting statistic and increases the relative standard error (RSE). The RSE in this study was up to 0.13‰ and up to 0.38‰ for δ^{56}Fe and δ^{57}Fe, respectively (Supplementary Table 6).

5. Sulfide petrography

Sulfide minerals occur as accessory phases in the studied lherzolite and wehrlite xenoliths, with narrower (0.005–0.03 with an average of ~0.01 vol%) and wider (0.005–0.07 with an average of ~0.03 vol%) modal ranges, respectively (Supplementary Table 2). The weakly metasomatized wehrlite xenoliths have lower (~0.02 vol%) sulfide contents compared to the moderately (~0.04 vol%) and strongly metasomatized (~0.03 vol%) wehrlite xenoliths (Supplementary Table 2). Sulfides are present in two textural positions: interstitial to or enclosed in rock-forming minerals. The interstitial sulfides are up to 500 μm in size with lobate boundaries and typically occur in triple-junctions among rock-forming minerals (Fig. 2a). The enclosed sulfides are usually isometric, rounded, or negative crystal-shaped with a size of 5–80 μm (Fig. 2b). The size of the texturally identical sulfides is similar in both the lherzolitic and the wehrlitic xenolith series. The enclosed sulfides have similar abundance in wehrlites compared to the lherzolites (29 and 27% of all sulfides, respectively) (Supplementary Table 2). The enclosed sulfides are hosted mostly in olivine or clinopyroxene, and rarely in orthopyroxene or spinel (Supplementary Table 2).

Sulfides consist of mss, pentlandite, pyrrhotite and chalcopyrite in various volume fractions (Fig. 3; Supplementary Table 3) formed by crystallization and exsolution during cooling. Mss and pentlandite are the most common in the lherzolite (Fig. 2c), whereas pyrrhotite (Fig. 2d) is more abundant in the wehrlite xenoliths. Pentlandite and pyrrhotite often show exsolution lamellae with a length of 2–4 μm after former mss in lherzolite xenoliths (Fig. 2e). Chalcopyrite typically appears on the rim of the sulfide grains in subordinate amount (dominantly <15 vol%) (Fig. 2f) and is usually slightly altered, forming iron hydroxide. Enclosed sulfides almost totally lack pyrrhotite in lherzolite xenoliths, however, it is a common phase in enclosed sulfides in the wehrlite xenoliths (Fig. 3b). In interstitial sulfides, pentlandite, mss and pyrrhotite are all present both in lherzolite and wehrlite xenoliths (Fig. 3a).

Rarely, small (up to 5 μm) sulfide inclusions are present along healed fractures close to host basalts, however, they were not considered in this study since they are usually linked to trails of secondary fluid and silicate melt inclusions (Supplementary Fig. 1a). These sulfide inclusions were likely trapped during the ascent of the host magma. In addition, some sulfides are completely altered to iron hydroxides, especially in host basalt-derived patches (Supplementary Fig. 1b) or along cracks (Supplementary Fig. 1c), which were not considered.

6. Sulfide geochemistry

6.1. Major elements

The major element compositions of different phases of sulfide grains in wehrlite and lherzolite xenoliths are summarized in Supplementary Table 4. Mss, pentlandite, pyrrhotite and chalcopyrite show minor differences in major element concentrations in lherzolite and wehrlite xenolith series. However, there is greater geochemical difference between sulfides occurring in different textural positions. On average, mss in interstitial sulfides shows slightly lower Fe (49.2 ± 5.1 wt%; hereafter standard deviation is 1σ), higher Ni (11.1 ± 4.9 wt%), and similar Co (0.16 ± 0.10 wt%) compared to mss in enclosed sulfides (51.0 ± 3.4; 9.3 ± 3.6 and 0.12 ± 012 wt%, respectively) independently of the xenolith lithology (Fig. 3). The largest difference is shown by pentlandite in enclosed sulfides, which is richer in Ni (32.3 ± 6.1 wt%), Co (0.68 ± 0.24 wt%), and more depleted in Fe (29.6 ± 4 wt% Fe) in the lherzolites

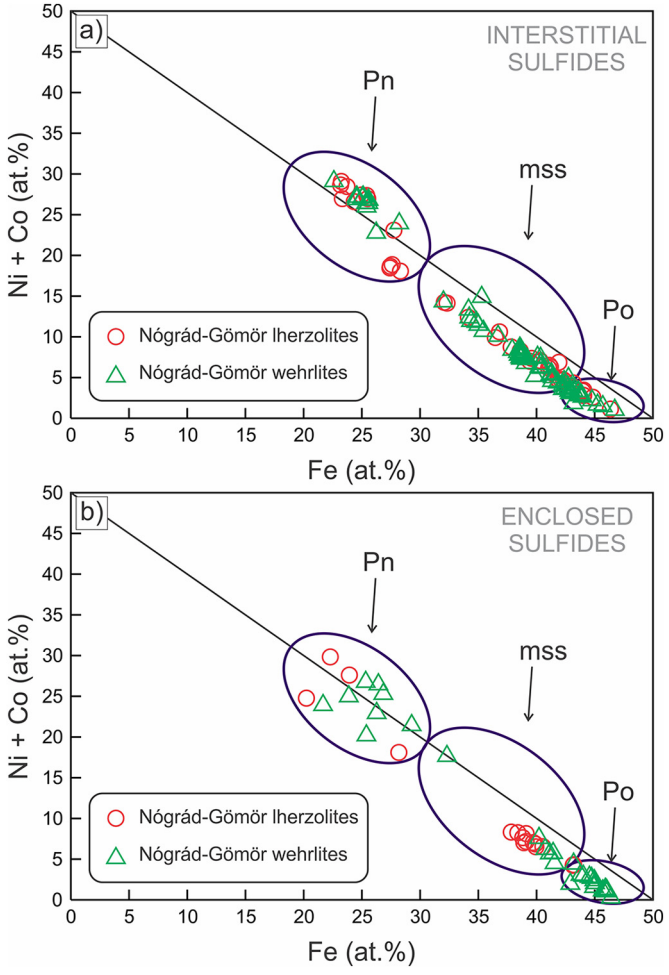

Fig. 3. Diagram of Fe (at. %) vs. Ni + Co (at. %) showing compositional ranges of pentlandite (pn), monosulfide solid solution (mss) and pyrrhotite (po) in **(a)** interstitial and **(b)** enclosed sulfides. Every symbol denotes an in situ data point. Modified after Szabó and Bodnar (1995).

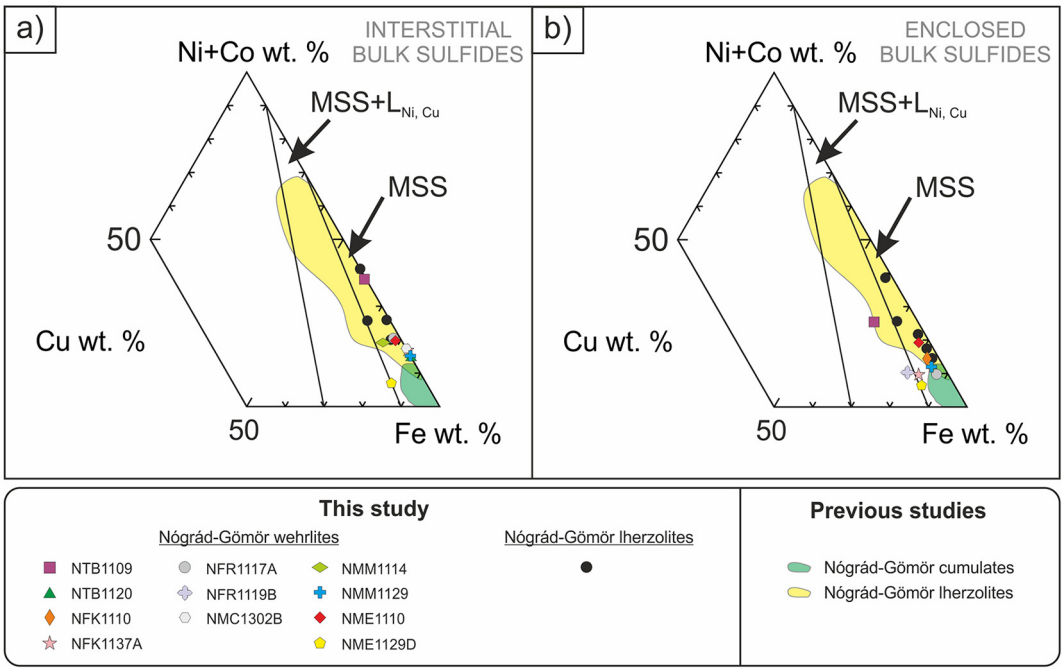

Fig. 4. Calculated bulk composition of **(a)** interstitial and **(b)** enclosed sulfides from the Nógrád-Gömör lherzolite and wehrlite xenoliths shown in the Cu-/Ni + Co/-Fe system. The stability relations were determined from the experiments of Craig and Kullerud (1969) carried out at 1000 °C and atmospheric pressure. The fields of the Nógrád-Gömör lherzolites and cumulates are from Szabó and Bodnar (1995) and Zajacz and Cs (2003). Mss and L_{Ni+Cu} denote the monosulfide solid solution and Ni- and Cu-rich liquid phase, respectively.

compared to the wehrlites (30.6 ± 2.7; 0.62 ± 0.26 and 31.7 ± 2.6 wt% for Fe, Ni and Co, respectively) (Fig. 3b).

We estimated the pre-cooling bulk compositions of the studied sulfides using mass-balance calculations (estimation based on the mineral composition of sulfides and chemical compositions of single sulfide phases) (Supplementary Table 2; Figs. 4 and 5). There are often significant variations (10–15 wt%) in the Fe and Ni content of sulfides even within a single xenolith. Generally, the lherzolitic sulfides are Fe-poor (46.4 ± 6.7 wt%) and Ni-rich (13.8 ± 6.2 wt%), in comparison with the wehrlitic ones (49.3 ± 6.6 and 9.5 ± 7.4 wt%, respectively). Furthermore, the Co content is higher (0.21 ± 0.13 wt%), whereas the Cu is lower (1.7 ± 1.7 wt%) in sulfides in the lherzolites compared to those in wehrlites (0.15 ± 0.10 and 2.7 ± 2.7 wt%, respectively). The average formulae of the sulfides are the following:

$Fe_{0.3633\pm0.0499}Ni_{0.1033\pm0.0469}Co_{0.0016\pm0.0010}Cu_{0.0122\pm0.0122}S_{0.5225\pm0.0136}$ for lherzolitic and $Fe_{0.3846\pm0.0484}Ni_{0.0714\pm0.0570}Co_{0.0011\pm0.008}Cu_{0.0190\pm0.0190}S_{0.5261\pm0.0152}$ for wehrlitic sulfides.

The interstitial sulfides have slightly lower Fe (48.1 ± 7.0 wt%) and somewhat higher Ni (11.6 ± 7.8 wt%) and Co contents (0.18 ± 0.13 wt%) than the enclosed ones (48.9 ± 5.9, 9.2 ± 5.5 and 0.16 ± 0.09 wt%, respectively) in both xenolith series (Figs. 4 and 5). The average formulae of the interstitial and enclosed sulfides, irrespectively of the lithology, are the following:

$Fe_{0.3759\pm0.0518}Ni_{0.0869\pm0.0600}Co_{0.0013\pm0.0009}Cu_{0.0146\pm0.0146}S_{0.5245\pm0.0163}$ for interstitial and $Fe_{0.3822\pm0.0442}Ni_{0.0688\pm0.0413}Co_{0.0012\pm0.007}Cu_{0.0218\pm0.0205}S_{0.5260\pm0.0099}$ for enclosed sulfides.

Enclosed sulfides have the same composition independently of the hosting phase (Supplementary Table 2).

The metal/sulfur ratio is slightly higher in lherzolitic (0.86–1.06 with an average of 0.92) than in wehrlitic sulfides (0.82–1.08 with an average of 0.90) (Fig. 6). This ratio shows no systematic difference between interstitial and enclosed sulfides (Fig. 6).

6.2. Trace elements

Trace element compositions of the studied sulfide minerals in two lherzolite (NTB1122, NME1116) and four representative wehrlite xenoliths (NTB1109, NTB1120, NME1129D, NME1110) are summarized in Supplementary Table 5.

Highly siderophile elements (HSE) exhibit a flat distribution for Ir-group platinum group elements (including Os, Ir, Ru) and Rh (Fig. 7). In contrast, Pt and partly, Pd show depletion with respect to the rest of the PGE. The Au contents in sulfides scatter dominantly around the CI chondrite value. The highly siderophile elements have similar concentration ranges in lherzolitic and wehrlitic sulfides (Fig. 7). The only exceptions are two analyses from sulfide grain number 2 in the lherzolite NTB1122/section 2, which show higher PGE concentrations compared to the rest of the sulfides, except for Os (Fig. 7.).

Tin and Ga, which are known for their siderophile, chalcophile and lithophile affinities, show dominantly lower concentrations compared to the CI chondrite values (Fig. 8). The lherzolitic and wehrlitic sulfides show similar compositional ranges in terms of these elements (Fig. 9).

Elements with both chalcophile-siderophile character (Re, Ge, Se, Te, As, Sb) mostly show higher values compared to the CI chondrite, with the exception of Ge (Fig. 8). Most of these elements have lower concentrations in the wehrlitic sulfides (Re: 0.05–1 with an average of 0.3 ppm; Ge: 1–5.9 with an average of 2.7 ppm; Se: 20–263 with an average of 65 ppm; Te: 0.6–62 with an average of 8.9 ppm) compared to the lherzolitic sulfides (Re: 0.4–0.5 with an average of 0.4 ppm; Ge: 2.8–5 with an average of 3.9 ppm; Se: 13–147 with an average of 102 ppm; Te: 3.2–64 with an average of 18 ppm) (Fig. 9). In contrast, Sb content is higher in wehrlitic (0.5–9.6 with an average of 3.2 ppm) than in lherzolitic sulfides (0.6–1.9 with an average of 1 ppm) (Fig. 9). Arsenic shows similar concentrations in sulfides of both xenolith series (Fig. 9).

Except for Zn, highly chalcophile trace elements (Ag, Cd, Pb, Tl, Bi) show generally higher values compared to the CI chondrite (Fig. 8). Most of these elements have higher concentrations in wehrlitic (Zn: 2.7–413 with an average of 61 ppm; Cd: 0.3–4.6 with an average of 2 ppm; Sb: 0.5–9.6 with an average of 3.2 ppm; Tl: 0.05–3.1 with an average of 0.8 ppm) compared to lherzolitic sulfides (Zn: 3.5–30 with an average of 15 ppm; Cd: 0.2–1.4 with an average of 0.8 ppm; Sb: 0.6–1.9 with an average of 1 ppm; Tl: 0.03–0.6 with an average of 0.2 ppm) (Fig. 9). Lead and Bi show similar concentrations in sulfides of both xenolith series (Fig. 9).

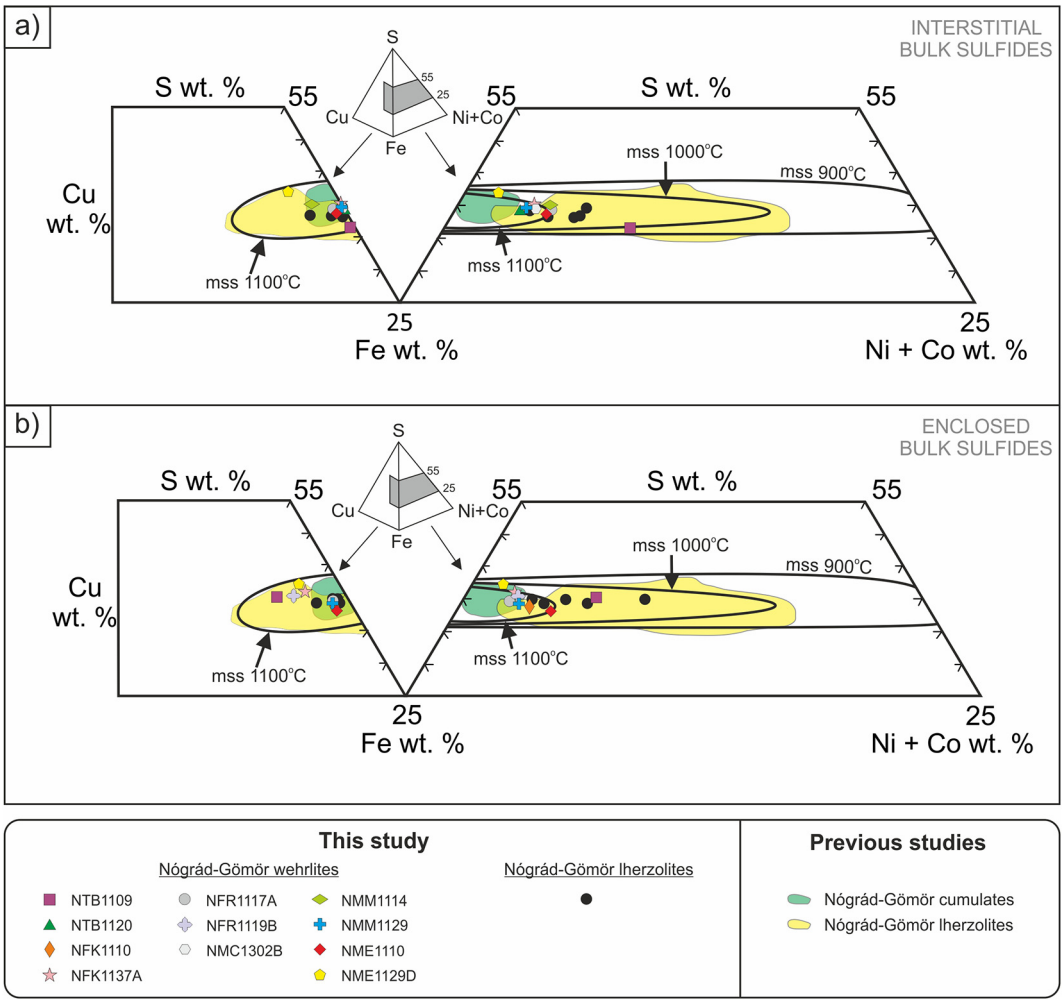

Fig. 5. Calculated bulk composition of **(a)** interstitial and **(b)** enclosed sulfides from Nógrád-Gömör lherzolite and wehrlite xenoliths shown in the Cu-S-Fe-/Ni + Co/ system at atmospheric pressure. The stability fields are based on the experiments of Kullerud et al. (1969). The fields of the Nógrád-Gömör lherzolites and cumulates are from Szabó and Bodnar (1995) and Zajacz and Cs (2003). Mss is the monosulfide solid solution.

6.3. Fe stable isotopes

In situ Fe stable isotopes (^{54}Fe, ^{56}Fe, ^{57}Fe) measurements have been carried out on sulfide grains from two lherzolite (NTB1122 and NME1116) and four wehrlite xenoliths (NTB1109, NTB1120, NME1110 and NME1129D) (Supplementary Table 6). The δ^{56}Fe values range from −0.13 to +0.56‰ (average: +0.10‰) and from −0.20 to +0.84‰ (average: +0.33‰), whereas δ^{57}Fe values are between

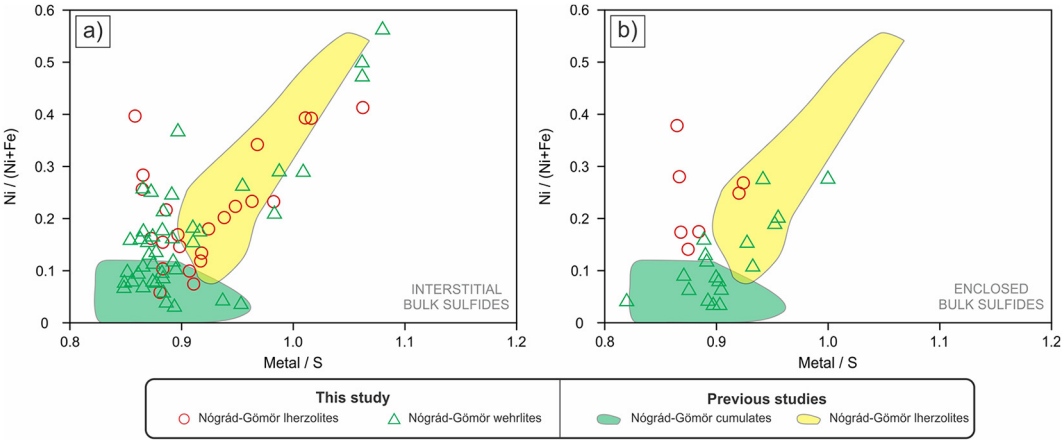

Fig. 6. Bulk metal/sulfur (Metal/S) vs. Ni/(Ni + Fe) for **(a)** interstitial and **(b)** enclosed individual sulfide grains, where bulk metal is the sum of Fe, Ni, Co and Cu. The fields of the Nógrád-Gömör lherzolites and cumulates are from Szabó and Bodnar (1995) and Zajacz and Cs (2003), respectively.

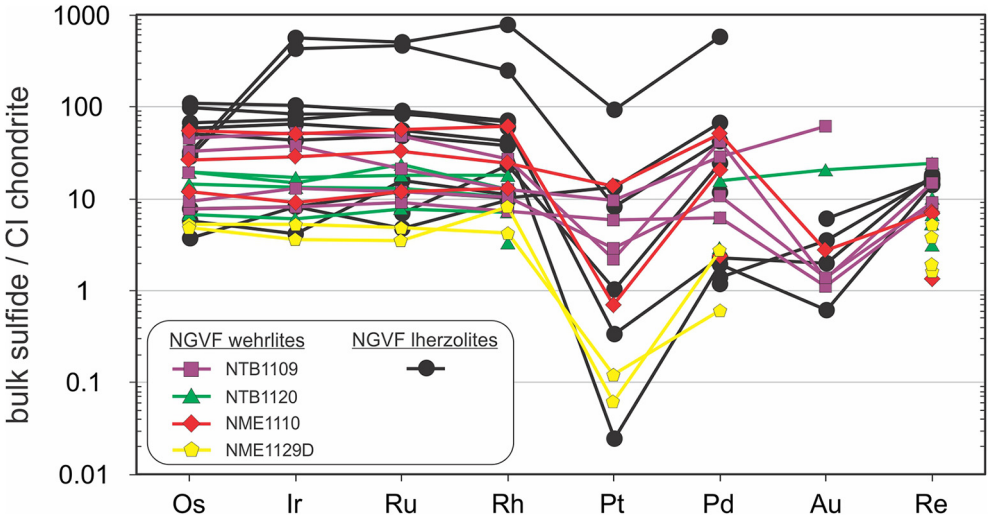

Fig. 7. Highly siderophile element patterns normalized to CI chondrite (McDonough and Sun, 1995) of bulk sulfides (with the exception for two, pentlandite- and pyrrhotite-dominated parts of a single sulfide (no. 7a in lherzolite NTB1122) with higher PGE concentrations; further information is in the Supplementary Table 5) in the Nógrád-Gömör lherzolite and wehrlite xenoliths.

−0.16 and + 0.76‰ (average: +0.14‰), as well as −0.26 and + 1.22‰ (average: +0.47‰) for lherzolites and wehrlites, respectively (Fig. 10). The Fe stable isotope signatures show no correlation with the bulk sulfide Fe contents (Supplementary Fig. 2). Based on the δ^{56}Fe data, sulfides in xenoliths collected from the NTB (Trebel'ovce) locality (NTB1122 lherzolite and NTB1109 and NTB1120 wehrlite xenoliths) have lower values (from −0.20 to +0.06‰ with an average of −0.08‰), whereas those from NME (Eresztvény) locality (NME1116 lherzolite and NME1110 and NME1129D wehrlite xenoliths) show higher values (from +0.56 to +0.84‰ with an average of +0.72‰) (Supplementary Table 6; Fig. 10).

7. Discussion

7.1. Physical and chemical characteristics of sulfide formation

Our petrographic and geochemical investigations were aimed at determining the origin of the sulfides in the NGVF xenoliths. Upper mantle sulfides may represent trapped grains in the residue after partial melting events (e.g. Luguet et al., 2007; Szabó and Bodnar, 1995) and/or sulfide melt drops crystallized during melt metasomatic events (e.g. Lorand et al., 2004; Wainwright et al., 2015). The textural distribution in the sulfides of the studied NGVF xenoliths shows no relationship with the host basalt or its infiltrations. It can also be noted that the enclosed and interstitial sulfides show similar geochemical characteristics in the investigated xenoliths (Fig. 4; 5), although the latter could potentially be modified by fluids and melts migrating along the grain boundaries. These observations indicate that all the studied sulfides were formed in the mantle before xenolith entrapment in the basalt and transport to the surface.

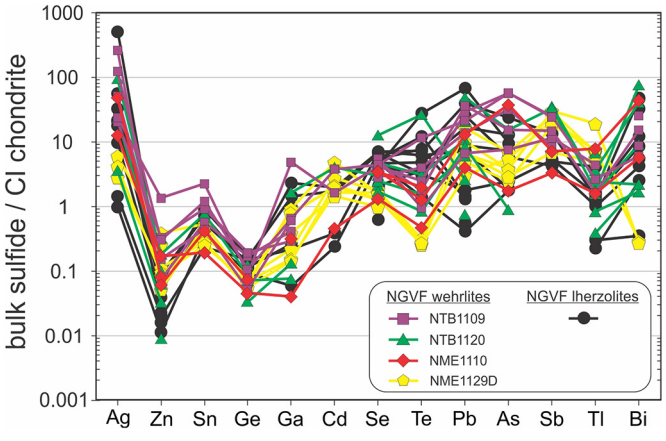

Fig. 8. Trace element patterns normalized to CI chondrite (McDonough and Sun, 1995) of bulk sulfides (with the exception for two, pentlandite- and pyrrhotite-dominated parts of a single sulfide (no. 7a in lherzolite NTB1122); further information is in the Supplementary Table 5) in the Nógrád-Gömör lherzolite and wehrlite xenoliths.

7.1.1. Origin of sulfides in lherzolite xenoliths

The evolution of the lherzolitic mantle beneath the NGVF is complex, with ancient depletion and subsequent multiple episodes of metasomatism (Liptai et al., 2017) that may imply complex evolution of the sulfides as well.

The two measured interstitial sulfide grains from the only Group IB member, metasomatized lherzolite xenolith (NFR0309), are not sufficient to define compositional fields. Both the interstitial and enclosed sulfide grains in Groups IA (depleted) and IIB (metasomatized) lherzolite xenoliths (Supplementary Table 2) have similarly wide composition ranges (Supplementary Figs. 3 and 4). The observed heterogeneity indicates that both residual, Fe-depleted (Ni + Co-rich) and metasomatized, Fe-enriched (Ni + Co-poor) sulfides can be found among both IA and IIB lherzolites. The variable trace element characteristics of the lherzolitic sulfides also indicate their complex origin (Figs. 9 and 12). Sulfides with different origin appear even within single lherzolite xenoliths (cf. Alard et al., 2000), which is further illustrated by PGE concentrations (Supplementary Table 5). The Ir-group platinum group elements (IPGE; including Os, Ir, Ru) are highly compatible, whereas the Pd-group platinum group elements (PPGE; including Pd, Pt, Rh) are less compatible (Luguet and Reisberg, 2016). Therefore, residual sulfides are expected to show subchondritic PPGE/IPGE, which is the case for 75% of the sulfide grains in lherzolite xenoliths (Supplementary Table 7). The major element composition of sulfides in lherzolites overlap with previously studied lherzolitic sulfides from the NGVF (Figs. 4, 5, and 11), which were also proposed to have formed dominantly during partial melting and occasionally by metasomatism (Szabó and Bodnar, 1995).

The chemically different sulfides appearing in lherzolite xenoliths can be divided into at least two populations. The first and larger

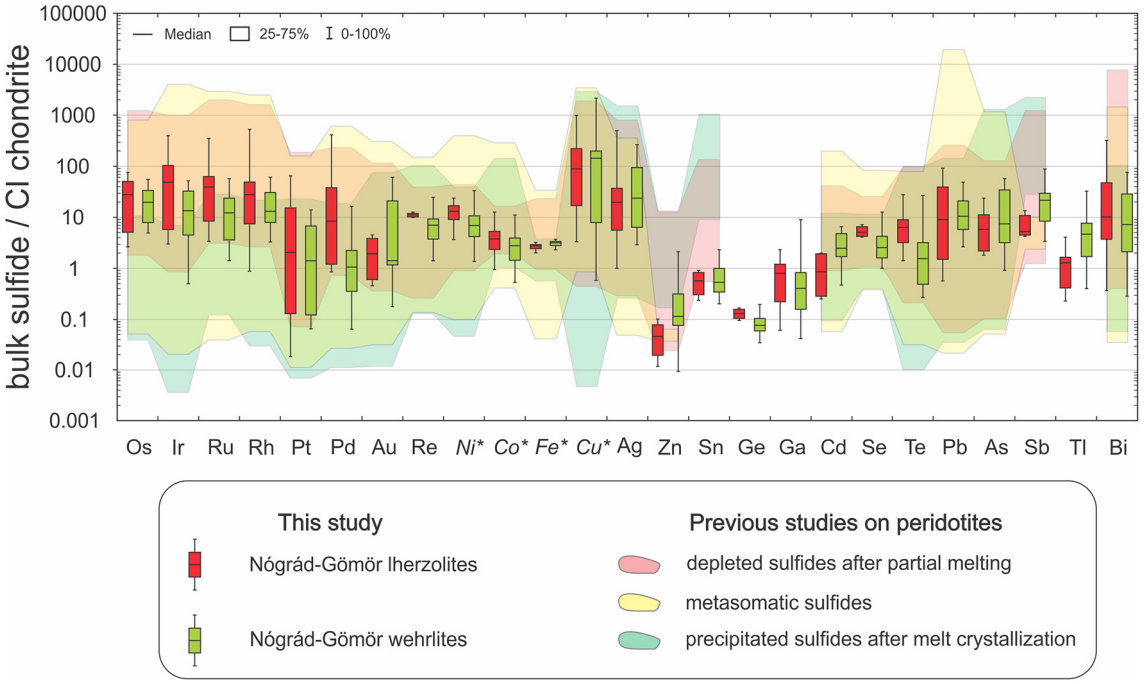

Fig. 9. Box and whisker diagrams of the CI chondrite-normalized (McDonough and Sun, 1995) major and trace elements of sulfide grains in the Nógrád-Gömör lherzolite and wehrlite xenoliths. Data of major elements (marked in italic and with asterisks) are based on calculated bulk sulfide results. The reference fields are based on in situ analyses of various bulk sulfide grains in peridotites: depleted sulfides (González-Jiménez et al., 2014; Guo et al., 1999; Saunders et al., 2015, 2016; Westner et al., 2019), metasomatic sulfides (Alard et al., 2011; Delpech et al., 2012; González-Jiménez et al., 2014; Saunders et al., 2015; Westner et al., 2019) and sulfides precipitated after melt crystallization (D'Errico et al., 2019; Guo et al., 1999; Saunders et al., 2016).

population is represented by residual sulfides formed after partial melting. The second, smaller population is linked to metasomatism, which was, however, not pervasive in contrast to the wehrlitization, which led to intensive overprinting of the modal and chemical composition of the precursor (Patkó et al., 2020). This suggests that sulfides from the various lherzolite groups represent a population which differs from sulfide population in wehrlite xenoliths. Thus, comparing lherzolitic to wehrlitic sulfides, which were formed by a single intensive metasomatic event, allows us to understand the metasomatic imprint on the metal budget.

7.1.2. Origin of sulfides in wehrlite xenoliths

Several lines of evidence support the idea that at least part of the identified sulfide grains in the wehrlite xenoliths were formed by the same metasomatic melt that modified the rock-forming mineral composition. These observations are: (1) the higher sulfide content of wehrlite (~0.03 vol%) compared to the precursor lherzolite xenoliths (~0.01 vol%) (Supplementary Table 2); (2) enclosed sulfides appearing dominantly (94%) in olivine and clinopyroxene in wehrlite xenoliths (Supplementary Table 2), which were both formed during the wehrlitization (Patkó et al., 2020); (3) the wehrlitic sulfides having higher bulk Fe and lower Ni and Co contents compared to the lherzolitic sulfides (Figs. 4, 5 and), which is consistent with the Fe enrichment of the rock-forming minerals (Patkó et al., 2020); (4) Fe- and Ni contents of the wehrlitic sulfides and silicates showing a positive and a negative correlation, respectively (Fig. 11); (5) pyrrhotites are in disequilibrium with ultramafic rocks due to their little Ni contents (dominantly <3 wt%; Fig. 3) (e.g. Lorand and Grégoire, 2006); (6) trace element trends of wehrlitic sulfides plotting in the field defined by sulfides crystallized from mafic melts (D'Errico et al., 2019; Guo et al., 1999; Saunders et al., 2016) (Fig. 12), which indicates that sulfide formation in wehrlite xenoliths is linked to a mafic melt.

The formation of sulfides during wehrlitization is related to the formation of minerals enriched in Fe (olivine, clinopyroxene) (Patkó et al., 2020), leading to Fe decrease and Si enrichment in the metasomatic melt. This resulted in lowering the S concentration at sulfide saturation (SCSS) (O'Neill and Mavrogenes, 2002). Additionally, the higher the pressure, the less S is needed for sulfide saturation (Mavrogenes and O'Neill, 1999). Wehrlite formation occurred at an estimated pressure of 1.3–1.6 GPa (Patkó et al., 2020), with a corresponding value for SCSS at around 1200 ppm S (Mavrogenes and O'Neill, 1999). Such S concentration is common in basaltic melts under upper mantle conditions (e.g. Jugo et al., 2005).

To determine the formation conditions of the wehrlitic sulfides, we estimated their equilibrium temperatures using the experimentally determined mss phase relations (Kullerud et al., 1969). The calculated bulk compositions of enclosed sulfides from the studied wehrlite xenoliths indicate higher temperatures (~1100–1150 °C) than what was determined for lherzolitic sulfides (~1050–1100 °C) (Fig. 5b). This is also confirmed by silicate-based thermometers (Liptai et al., 2017; Patkó et al., 2020).

To further constrain the formation conditions of wehrlitic sulfides, we compared their geochemical data with sulfides from the Nógrád-Gömör cumulate xenoliths (Zajacz and Cs, 2003). The cumulates (clinopyroxenites and plagioclase-bearing ultramafic rocks) crystallized from basaltic melts accumulated immediately under the Moho during the Neogene alkali basaltic volcanic event (Kovács et al., 2004; Zajacz et al., 2007). Note that the cumulates were all sampled from the central part of the NGVF, which coincides with the area of wehrlite formation (Fig. 1b).

The wehrlitic sulfides fall between the fields of the Nógrád-Gömör lherzolites (Szabó and Bodnar, 1995) and cumulates (Zajacz and Cs, 2003) in the Cu-/Ni + Co/-Fe, Cu-S-Fe and Fe-S-/Ni + Co/ systems (Figs. 4 and 5). Furthermore, the geochemical evolution of wehrlitic sulfides, using coexisting sulfide and silicate minerals, points towards the

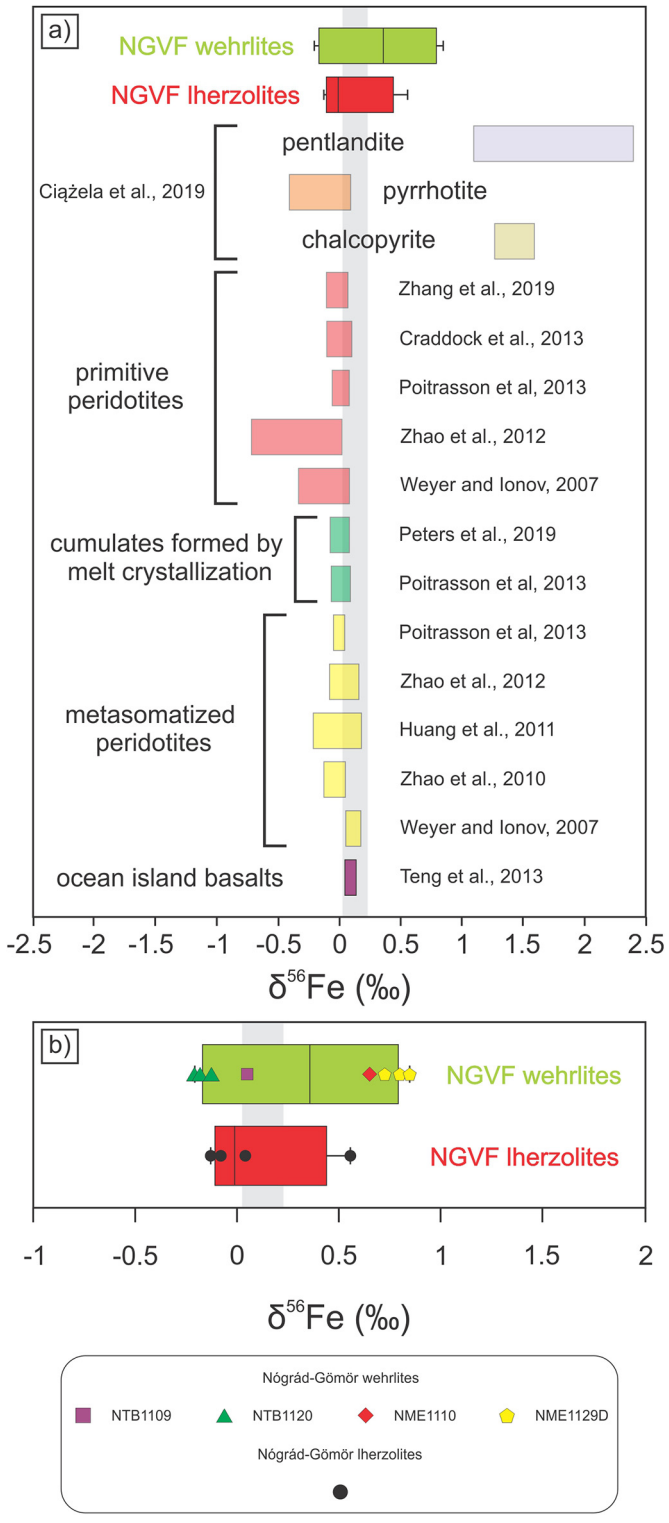

Fig. 10. δ^{56}Fe signatures of sulfide grains from the Nógrád-Gömör lherzolite and wehrlite xenoliths with respect to reference data. Solid black lines within the lherzolite and wehrlite boxes indicate the median value. The grey field represents the value range for the terrestrial mantle (Craddock et al., 2013). Data from Ciążela et al. (2019) refer to in situ analyses of pentlandites pyrrhotites and chalcopyrites from gabbros of the lower oceanic crust. The rest of the results refer to bulk rocks.

field of the Nógrád-Gömör cumulates (Fig. 11). The similar chemical compositions of sulfides in the wehrlite and cumulate xenoliths suggest their cognate formation. It is suggested that sulfides in both the wehrlite and cumulate xenoliths are related to migrating and crystallizing mafic melts leading to higher Fe and lower Ni and Co contents in them.

Consequently, the wehrlitic sulfides represent an assemblage formed in the same magmatic system as the one forming the cumulative sulfides, but at greater depth.

7.2. The effect of wehrlitization on siderophile and chalcophile element budget

The higher modality of sulfide in wehrlite xenoliths (Supplementary Table 2) suggests that S was added to the bulk rocks during the melt-wall rock interaction. The higher S fugacity of the metasomatizing melt is further supported by the lower metal/S ratio in wehrlitic sulfides with respect to the lherzolitic sulfides (Fig. 6). As stated above, wehrlitization resulted in Fe enrichment and relative Ni—Co depletion both in the sulfides and in the rock forming silicates (Fig. 11). These trends are broadly known from silicates of mafic melt-metasomatized peridotites (e.g. Peslier et al., 2002; Patkó et al., 2020). However, our knowledge on the behavior of siderophile and chalcophile elements during such melt metasomatism is limited, and mostly restricted to PGEs (Büchl et al., 2002; Luguet et al., 2008) or to the oceanic (Ciążela et al., 2017, 2018) or cratonic lithosphere (Aulbach et al., 2021).

The patterns of highly siderophile PGE obtained from the wehrlitic sulfides are quite similar to those from the lherzolitic sulfides (Fig. 7). The only exceptions are two lherzolitic sulfide grains from xenolith NTB1122 with higher Ir, Ru, Rh, Pt and Pd contents compared to the rest of the analyses (Fig. 7). This is because they only include the pentlandite or pyrrhotite parts of the sulfide, whereas the rest of the analyses represent polyphase bulk sulfides. The similar element concentrations in sulfides from the wehrlitic and lherzolitic sulfides (Fig. 7) may indicate that the metasomatic melt could not mobilize the highly siderophile elements, and that the PGE content of the wehrlitic sulfides was inherited from the precursor lherzolite sulfides. However, similar PGE concentrations in single sulfide grains of the two xenolith series (Fig. 7) indicate higher bulk rock PGE contents and thus enrichment in the wehrlite xenoliths due to their higher sulfide modal proportions (Supplementary Table 2).

In contrast, trace elements with both chalcophile and siderophile character show different concentrations for lherzolitic and wehrlitic sulfides: Re, Ge, Se and Te are more depleted, whereas Sb is more enriched in wehrlitic compared to lherzolitic sulfides (Figs. 9 and 12). These elements prefer to partition in pentlandite which represents a refractory mantle component (Garuti et al., 1984), and, to a lesser extent, they are incorporated in pyrrhotite or chalcopyrite (Aulbach et al., 2021; Ciążela et al., 2018) (Fig. 12.). This suggests that these elements have relatively low affinity to sulfur, and thus are diluted in Fe-rich silicate melts such as the wehrlitizing melt beneath the NGVF (Patkó et al., 2020), which may explain their lower concentration in wehrlitic sulfides (Fig. 9). A decrease in bulk Re concentration linked to basaltic melt percolation (Figs. 9 and 12) was also observed in mantle xenoliths from east central China (Reisberg et al., 2005). This suggests that the interaction of ultramafic rocks with basaltic melts results in low Re concentrations in the newly formed sulfides. Consequently, the concentration of Re correlates ($r^2 = 0.79$) negatively with the S/Se ratio (Fig. 12g), which is a widely applied indicator of metasomatism. Since S is preferentially transported in the melt whereas Se is more compatible, metasomatized peridotites are generally characterized with high S/Se (Alard et al., 2011). The high concentrations of Sb in wehrlitic sulfides are most likely related to the geochemical character of the metasomatic melt.

Highly chalcophile elements such as Cu, Zn, Cd, and Tl show higher concentrations in wehrlitic than lherzolitic sulfides (Figs. 9 and 12). Copper, Zn and Cd are dominantly incorporated in chalcopyrite (Ciążela et al., 2018) which is more abundant in wehrlitic than in lherzolitic sulfides, and thus wehrlitic sulfides become enriched in Cu, Zn and Cd. Since minor amount (i.e. few tens of ppm) of these elements

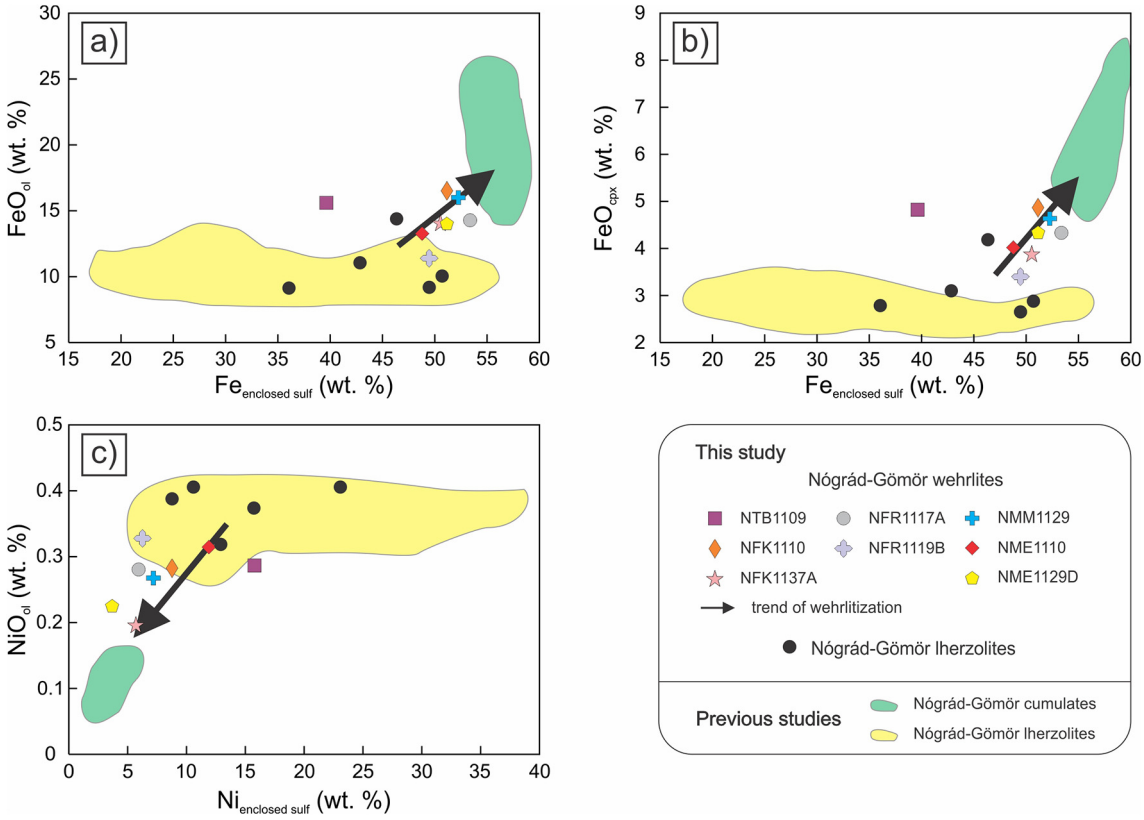

Fig. 11. Relationship between **(a)** Fe in enclosed bulk sulfides vs. FeO in olivines **(b)** Fe in enclosed bulk sulfides vs. FeO in clinopyroxenes **(c)** Ni in enclosed bulk sulfides vs. NiO in olivines. Data points represent weighted average per sample. The arrows indicate the wehrlitization trends. The fields for the Nógrád-Gömör lherzolite and cumulate xenoliths are from Szabó and Bodnar (1995) and Zajacz and Cs (2003), respectively.

can also reside in clinopyroxene, its higher modal proportion in wehrlite xenoliths suggests even more significant Cu-Zn-Cd enrichment in the wehrlite bulk rock. In contrast, Tl is related to pyrrhotite (cf. Ciążela et al., 2018), which is the most abundant mineral in the wehrlitic sulfides. Thallium may thus be linked to the Fe-rich metasomatic melt. The rest of the highly chalcophile elements (Ag, Pb, Bi) show no observable difference between the various lithologies (Fig. 9).

Tin and Ga, which have lithophile affinity in addition to their chalcophile and siderophile character, have a complex behavior and show no compositional change linked to the wehrlitization (Fig. 9).

In summary, wehrlitization affected the concentration of several metals. Metals that are both chalcophile and siderophile are depleted, whereas highly chalcophile metals are enriched in wehrlitic sulfides. The former show high affinity to pentlandite, which is less frequent in wehrlitic sulfides, whereas the latter are preferentially incorporated into pyrrhotite and chalcopyrite, which have higher mode in wehrlitic sulfides with respect to the lherzolitic sulfides (Fig. 3). PGEs show no systematic change between single sulfide grains of the two xenolith series, which implies an enrichment in the wehrlite bulk rock due to the higher sulfide modal proportion in these rocks.

7.3. Relationship between the degree of metasomatism and sulfide geochemistry

The wehrlite xenoliths of the NGVF were classified into three groups (i.e. strongly, moderately and weakly metasomatized) depending on the degree of metasomatism recorded by the Mg# of the silicates and Cr# (Cr/[Cr + Al]) of the spinels (Patkó et al., 2020). Accordingly, the strongly metasomatized wehrlite xenoliths have Mg# < 0.86 in olivine, Mg# < 0.86 in clinopyroxene and Cr# < 0.20 in spinel, whereas the weakly metasomatized wehrlite xenoliths have Mg# > 0.87 in olivine; Mg# > 0.88 in clinopyroxene and Cr# > 0.19 in spinel.

The weakly metasomatized wehrlite xenoliths have lower (~0.02 vol%) sulfide contents compared to the moderately (~0.04 vol%) and strongly metasomatized (~0.03 vol%) ones (Supplementary Table 2). This suggests that the low melt/rock ratio (<0.3) characteristic for the weakly metasomatized wehrlites is associated with less sulfides, whereas the high melt/rock ratio (>0.3) typical to strongly metasomatized wehrlites is accompanied with more sulfides.

The average major element composition of the interstitial and enclosed sulfides in wehrlite xenoliths in the Cu-/Ni + Co/-Fe and Cu-S-Fe-/Ni + Co/systems form a cluster with the exception of those in the least metasomatized xenolith NTB1109 (Figs. 4 and 5). The averaged interstitial and enclosed sulfides of NTB1109, characterized by high Ni + Co content, overlap with the field defined by the lherzolitic sulfides (Szabó and Bodnar, 1995) (Figs. 4 and 5). On sulfide-silicate relation plots, data points of this xenolith consequently fall around the starting point of the wehrlitization trends and overlap with the lherzolitic fields (Fig. 11). In contrast, the strongly metasomatized wehrlite xenoliths (NFK110, NFR1117A, NMM1129) plot at the end of the wehrlitization trends, close to the field of sulfides from cumulates defined by Zajacz and Cs (2003) (Fig. 11), and the same observations can be made in the Cu-/Ni + Co/-Fe (Fig. 4) and Cu-S-Fe-/Ni + Co/ (Fig. 5) systems. The wehrlite xenoliths, whose sulfides were subjected to trace element measurements, cover the entire spectrum from weakly (NTB1109), through moderately (NME1110, NME1129D), to strongly (NTB1120) metasomatized samples. Sulfides in the moderately and strongly metasomatized wehrlites have higher Zn and Sb, as well as lower Re, Ge, Se and Te contents compared to those are situated in the weakly metasomatized werhlite (Fig. 12). All these observations suggest that the degree of metasomatism and related redistribution of rock forming minerals also influences the geochemistry of sulfides.

Even though the wehrlitization resulted in significant sulfide enrichment, ~25% of the current sulfide inventory is inherited from the

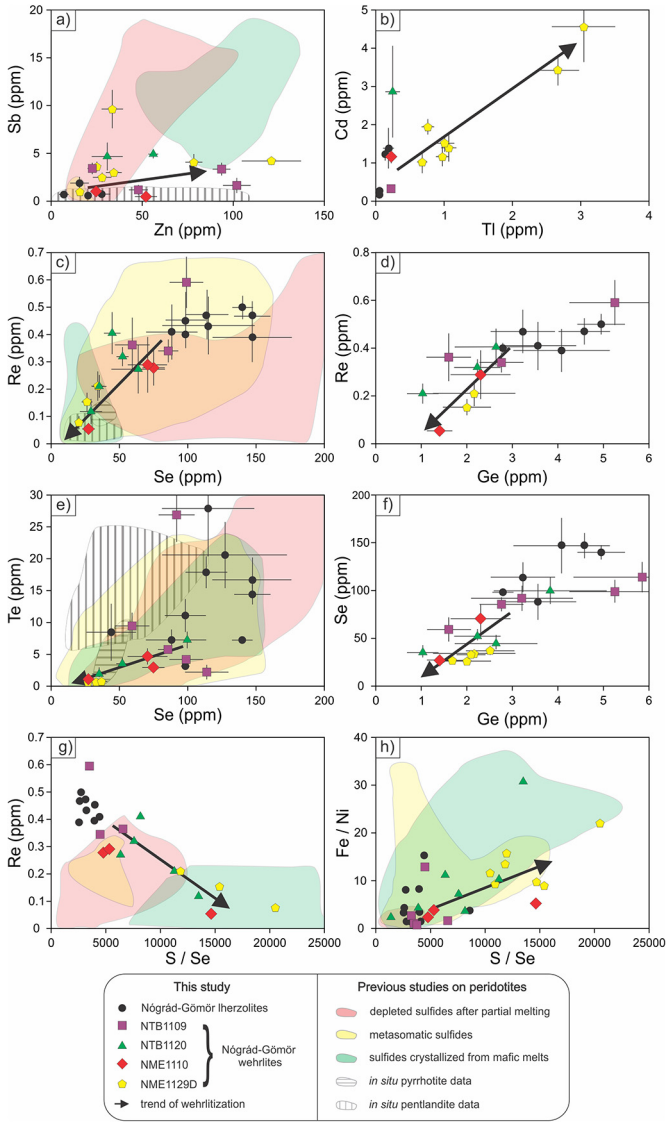

Fig. 12. Scatterplots comparing trace element contents in sulfide grains of the Nógrád-Gömör lherzolite and wehrlite xenoliths. Red, yellow, and green reference fields are based on in situ analyses of various sulfide grain populations in peridotites: depleted sulfides (González-Jiménez et al., 2014; Guo et al., 1999; Saunders et al., 2015, 2016; Westner et al., 2019), metasomatic sulfides (Alard et al., 2011; Delpech et al., 2012; González-Jiménez et al., 2014; Saunders et al., 2015; Westner et al., 2019), sulfides precipitated after melt crystallization (D'Errico et al., 2019; Guo et al., 1999; Saunders et al., 2016). In situ pentlandite and pyrrhotite data are from the studies of Aulbach et al. (2019, 2021).

precursor lherzolites and these are still present alongside the newly formed metasomatic sulfides (Fig. 13), as suggested by sulfides in wehrlites having geochemical characteristics similar to those from lherzolitic sulfides (Fig. 12). This variability suggests that sulfides in different areas within single xenoliths were affected by the wehrlitization process to different extent, similarly to the silicates (Patkó et al., 2020).

7.4. Iron isotope systematics of lherzolitic and wehrlitic sulfides

Iron isotopes have been studied in bulk rocks of the upper mantle peridotites and in situ in their rock forming minerals (Peters et al., 2019 and references therein). However, in situ Fe isotope analyses of upper mantle sulfides are scarce (Ciążela et al., 2019).

The wehrlitic sulfides show wide δ^{56}Fe range (from −0.20 to +0.84‰) with several sulfide grains having quite heavy Fe isotope compositions (> + 0.6‰) (Fig. 10). In contrast, the lherzolitic sulfides have less variable and generally lighter δ^{56}Fe values (from −0.13 to +0.56‰) (Fig. 10).

The general trend seems to indicate that the metasomatism caused enrichment in heavier Fe isotopes. However, irrespectively to the xenolith lithology, there is a significant difference between the δ^{56}Fe results of sulfides from the two sampling localities (NTB: from −0.20 to +0.04‰; NME: from +0.56 to +0.84‰; Supplementary Fig. 5; Supplementary Table 6). This suggests that local variations of isotopic signatures were not entirely overprinted by the wehrlitization process.

Pentlandite, pyrrhotite and chalcopyrite show different δ^{56}Fe values (Fig. 10a), thus the variable δ^{56}Fe values of the studied sulfides can reflect modal characteristics. Pyrrhotite dominates the wehrlitic sulfides, whereas pentlandite and mss prevails the lherzolitic sulfides in both the xenolith from Trebeľovce (NTB) and the one from Eresztvény (NME). This suggests that it is not the modal proportion of these minerals that determines the isotope differences between these localities. Chalcopyrite is a common mineral both in the wehrlitic (appears in ~75% of the sulfides) and lherzolitic sulfides (appears in ~60% of the sulfides) from the NME locality. In contrast, it is rare in the NTB locality (appears in ~25% of both the wehrlitic and lherzolitic sulfides). Since chalcopyrite is characterized by heavy δ^{56}Fe values (from +1.28 to +1.60‰; Fig. 10a), its higher abundance in the NME xenoliths can explain the heavier isotope characteristics (Fig. 10a). Heavy isotopes prefer lattice sites with low coordination (high-bonding energy) (Urey, 1947). The coordination number of Fe is lower in chalcopyrite (2), than in pyrrhotite (4) and pentlandite (4), which can explain the heavier Fe isotope characteristics in chalcopyrite with respect to the latter two. This also suggests that the type of mineral that crystallizes might be the dominant control on isotope systematics of sulfides and can veil the isotopic composition of the metasomatic melt agent. These findings are in agreement with the results of Polyakov and Soultanov (2011), who studied the Fe β-factors of sulfides and predicted at equilibrium the isotope ratio of the substance of interest with respect to the isotope ratio of dissociated atoms. They concluded that the higher β-factor (0.5) for chalcopyrite compared to troilite (0.3) can explain the heavy Fe isotope enrichment in chalcopyrite. The reason why sulfides in the NME locality are richer in Cu can be the high temperature (>800 °C) differentiation of the sulfide melt (c.f. Lorand and Grégoire, 2006). This local phenomenon could have happened due to the crystallization of mss (~1200–1000 °C) and the subsequent formation of a Cu-rich liquid, which solidifies as iss (intermediate solid solution) at lower temperature (900–800 °C) (Mansur et al., 2021).

The reason why the wehrlitization was not accompanied by Fe isotope fractionation that would have resulted in Fe isotope differentiation between wehrlitic and lherzolitic sulfides is questionable.

One possible explanation can be the similar Fe isotopic composition of the metasomatic agent and the precursor lherzolite. The NGVF wehrlites were formed by contribution of an OIB-like melt which is assumed to be homogenous underneath the entire volcanic field (Patkó et al., 2020). OIB-like melts typically have a narrow δ^{56}Fe range (from +0.05 to +0.14‰; Teng et al., 2013) (Fig. 10). Note that there is only one wehrlitic sulfide whose δ^{56}Fe value is within the range defined by OIB-like melts (Fig. 10b). Assuming that OIB melts have similar Fe isotopic compositions worldwide, the original Fe isotope composition of the metasomatic agent does not determine the Fe isotope characteristics of the wehrlitization, possibly because of its compositional change related to the melt-wall rock interaction (e.g. incorporation of sulfides occur in the precursor). This precludes the isotopic equilibrium between the melt agent and the precipitated sulfides leading to wide Fe isotopic ranges in wehrlitic sulfides (Fig. 10b).

Magma differentiation usually does not affect δ^{56}Fe in basaltic systems (e.g. Schuessler et al., 2009). However, constant bulk δ^{56}Fe during melt differentiation may result from the contrasting effect of various

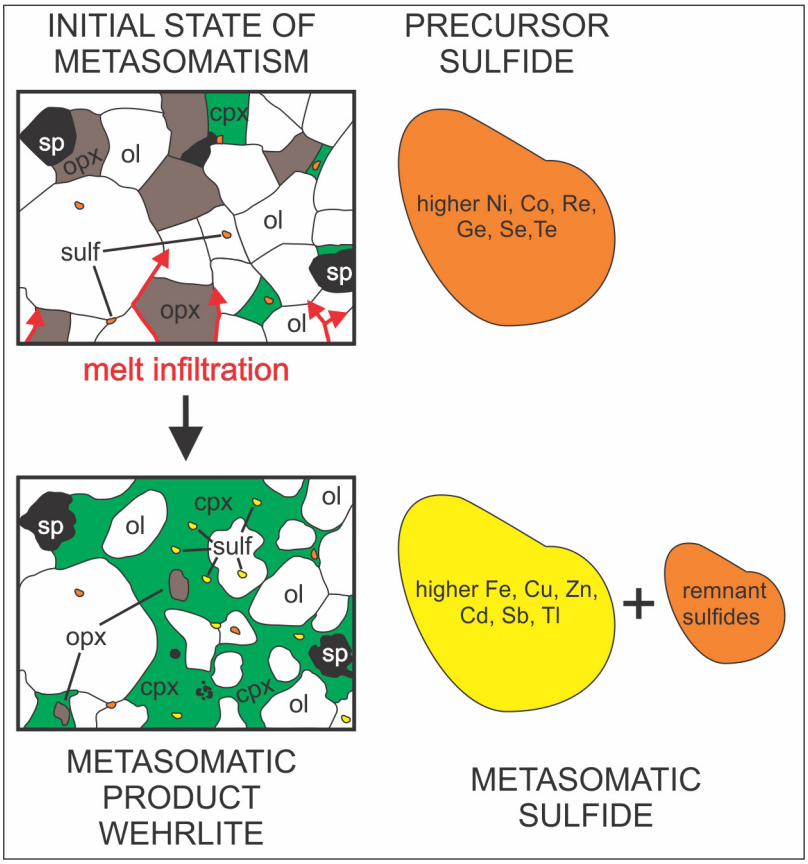

Fig. 13. Schematic model of the wehrlitization process (adapted from Patkó et al., 2020) with emphasis on sulfides. Geochemical characteristics of the precursor (orange) and metasomatic (yellow) sulfides are highlighted on the right side. Abbreviations: ol - olivine, opx - orthoproxene, cpx - clinopyroxene, sp. - spinel, sulf - sulfide.

crystallizing minerals. For example, the simultaneous fractionation of olivine (preferring lighter Fe isotopes) and spinel (preferring heavier Fe isotopes) results in neutral δ^{56}Fe signature in the melt (McCoy-West et al., 2018). The interaction of peridotites and silica-undersaturated melts produces metasomatized lherzolites or wehrlites with heavier δ^{56}Fe signatures, as it was observed both in lherzolites (from +0.15 to +0.19‰; Huang et al., 2011) and wehrlites (from +0.01 to +0.17‰; Weyer and Ionov, 2007; Zhao et al., 2010, 2012). This suggests that changes in clinopyroxene modal volume, which is a common mineral during such metasomatic reactions, likely plays a key role in Fe isotope fractionation. In fact, Zhao et al. (2010) concluded that the higher the clinopyroxene content of the metasomatic product, the heavier the bulk Fe isotope composition. In the NGVF wehrlites, clinopyroxene, and to a lesser extent, olivine, crystallized at the expense of orthopyroxene (Patkó et al., 2020). Therefore, it is likely that olivine and clinopyroxene formation have contrasting effects on the Fe isotope fractionation during wehrlitization, as witnessed in the sulfides.

Kinetic fractionation, which would lead to lighter isotope signatures in the wehrlites (Teng et al., 2011) is significant only for low melt/rock ratio (<0.1; Poitrasson et al., 2013). However, this is not the case during NGVF wehrlite formation, where melt/rock ratio was estimated between 0.2 and 0.4 (Patkó et al., 2020). Furthermore, according to Zhang et al. (2020), in case of kinetic iron isotopic fractionation, the Fe content correlates negatively with δ^{56}Fe, which was not observed in the wehrlitic sulfides (Supplementary Fig. 2).

As a summary, we suggest that none of the mentioned factors (melt agent isotopic characteristics, isotope fractionation due to magma differentiation, kinetic fractionation) was dominant enough to control Fe isotope fractionation. Therefore, the Fe isotope composition of the melt was likely buffered by the local lherzolitic rocks, resulting in balanced Fe isotope composition in the lherzolites and wehrlites.

7.5. Sulfide enrichment in the upper mantle as a global process

In recent years, sulfide minerals enrichment has been reported or inferred along oceanic crust-mantle transition zones (Ciążela et al., 2017, 2018; González-Jiménez et al., 2020), which may indicate a global metal enrichment along the oceanic Moho. This seems to be confirmed by copper deposits found in crust-mantle transition zones in ophiolites (e.g. Panayiotou, 1978). Although a similar phenomenon was recognized along the subcontinental crust-mantle boundary (e.g. Chen et al., 2020), there are only a few studies focusing on the migration of chalcophile elements (e.g. Blanks et al., 2020), due to scarcity of suitable exposures (Moho is on average ~ 35 km below the continent surface and is rarely exposed tectonically) (e.g. Grad et al., 2009). Nevertheless, preliminary studies in orogenic peridotite massifs reveal sulfide enrichment along peridotite-gabbro contacts in pressure conditions comparable to the continental Moho (0.5–1 GPa) (Pieterek et al., 2019), although the precipitation of sulfides during melt-peridotite interaction seems to occur independently of the pressure. This is supported by the fact that sulfides are present both at low pressures (0.1–0.2 GPa) at the oceanic crust-mantle transition zones (Negishi et al., 2013), as well as at high pressures (up to 2.5 GPa), which is more comparable to the environment of mantle xenoliths (e.g. Lorand et al., 2003; Wang et al., 2009). The elevated sulfide modes in metasomatic rocks represented by our wehrlite xenoliths demonstrate that the upper continental mantle is fertilized by ascending melt. Hence, large portion of S and associated chalcophile elements rather remain

in the continental mantle and do not reach the crust, as has been previously proposed for the oceanic (Ciążela et al., 2017) and cratonic lithosphere (Aulbach et al., 2021). The observed process may occur at various depths in the continental mantle; for example, the NGVF xenoliths record pressures of 1.3–1.6 GPa (Patkó et al., 2020). The intensity of this process is likely even greater below the Moho, as evidenced by orogenic massifs where peridotites are in contact with gabbros (Pieterek et al., 2019).

The refertilization of the mantle with metals during melt-wall rock reaction at the crust-mantle transition and along melt channels in the upper mantle may influence the local, regional, and potentially, the global metal mass balance of the continental lithosphere. A Cu deficit in the lower oceanic crust was already highlighted by Ciążela et al. (2018), who argued that 20–62% of the Cu load of a primitive melt could be retained below the crust, namely, at the oceanic crust-mantle transition or in melt-modified mantle rocks of the upper mantle. The remobilization of mantle sulfides by sulfide-undersaturated melts (Aulbach et al., 2021) or by buoyant CO_2 bubbles (Blanks et al., 2020) can contribute to porphyry and related epithermal mineral deposits (Sillitoe, 2010). Our study indicates that sulfide enrichment, likely to a lesser extent, occurs in the upper continental mantle, and potentially, in the continental crust-mantle transition zone. However, although our observation is well-documented and quantitative due to the in situ investigation of sulfides, more studies are needed to estimate the effect of this process on the global mass balance at the continental lithosphere. In addition, we assume that further systematic studies of peridotite-gabbro contacts from continental crust-mantle transition zones will prove useful in the future. One of the most important questions that remain is the quantitative significance of S and metal loss along melt channels in the upper mantle and presumably in larger-scale zones at the crust-mantle boundary, where melts may stagnate due to the lower density of the overlying crust and interact with the mantle for a longer time.

8. Conclusions

1. The alkali basalt-hosted upper mantle xenoliths of Nógrád-Gömör Volcanic Field are classified into a lherzolitic and wehrlitic series. We compared sulfides from both the lherzolite and the wehrlite xenoliths. Sulfides are more abundant in wehrlites (~0.03 vol%) and often appear in enclosed textural positions, whereas those in lherzolites (~0.01 vol %) are dominantly interstitial. Monosulfide solid solution (mss) and pentlandite are the most common sulfide phases in lherzolites, whereas pyrrhotite is the most frequent in wehrlites.

2. Wehrlitic sulfides show higher bulk Fe and Cu, but lower bulk Ni and Co contents compared to the lherzolitic sulfides. The Fe-rich character of the wehrlitic sulfides agrees with the Fe enrichment trend in the wehrlitic rock forming minerals. This suggests that both the sulfides and rock forming minerals were affected by the same metasomatic event. The sulfides in wehrlites are enriched in highly chalcophile (Zn, Cd and Tl) and relatively depleted in simultaneously chalcophile and siderophile (Ge, Se, Te and Re) trace elements compared to the sulfides in the lherzolites. This suggests that the chalcophile affinity exerts the most decisive control on metal behavior during metasomatism. The similar S and PGE compositions in single lherzolitic and wehrlitic sulfides suggests moderate enrichment of these elements in bulk rock wehrlites due to their higher sulfide content.

3. The δ^{56}Fe signatures indicate isotopic fractionation between lherzolites and wehrlites with heavier isotope compositions in the wehrlitic sulfides. However, irrespectively to xenolith lithology, there is a significant difference between the δ^{56}Fe results of sulfides in the two studied sampling localities (NTB and NME). This suggests that local variations of isotopic signatures are not fully overprinted by the wehrlitization process. The δ^{56}Fe difference between the two xenolith localities is probably due to the higher chalcopyrite content in sulfides of the NME xenoliths compared to those of the NTB xenoliths.

4. Our results indicate that sulfide mineral and chalcophile element enrichment is a result of mafic melt metasomatism in the subcontinental lithospheric mantle. We showed that part of the copper and other chalcophile metals missing in the budget of the crust may have been retained in the mantle due to melt – wall rock interactions and never reached the crust.

Declaration of Competing Interest

None.

Acknowledgements

The authors would like to thank to the people who supported this study. Zsolt Bendő, Zoltán Kovács and Ábel Szabó are thanked for helping with the SEM analyses at the Eötvös Loránd University. We are grateful to Bernardo Cesare, Anna Maria Fioretti and Raúl Carampin for their help with the EMPA analyses at CNR Institute for Geosciences and Earth Resources (IGG) in Padua, Italy. Last but not least, we acknowledge Ingo Horn's help to set up the fs-LA-ICP-MS measurements at the Leibniz Universität Hannover. Xianhua Li is thanked for his editorial handling and useful suggestions, Sonja Aulbach and an anonym reviewer are thanked for their constructive comments and thorough structural shaping of the paper.

This research was funded by the National Science Centre Poland (PRELUDIUM 12 no. 2016/23/N/ST10/00288) to J. Ciążela, the MTA EK Lendület Pannon LithH_2Oscope Grant (LP2018-5/2018) to I.J. Kovács, and the Hungarian Science Foundation (OTKA, 78425) to Cs. Szabó. L. Patkó was supported by the GINOP-2.3.2-15-2016-00009 research program. The work of L. Patkó, L.E. Aradi, and Cs. Szabó was funded by the Eötvös Loránd University (ELTE) Institutional Excellence Program (TKP2020-IKA-05) supported by the Hungarian Ministry of Human Capacities. This is the 105th publication of the Lithosphere Fluid Research Lab (LRG).

Appendix A. Supplementary data

Supplementary data to this article can be found online at https://doi.org/10.1016/j.lithos.2021.106238.

References

Alard, O., Griffin, W.L., Lorand, J.P., Jackson, S.E., O'Reilly, S.Y., 2000. Non-chondritic distribution of the highly siderophile elements in mantle sulphides. Nature 407, 891–894.

Alard, O., Lorand, J.P., Reisberg, L., Bodinier, J.L., Dautria, J.M., O'reilly, S.Y., 2011. Volatile-rich metasomatism in Montferrier xenoliths (Southern France): Implications for the abundances of chalcophile and highly siderophile elements in the subcontinental mantle. J. Petrol. 52, 2009–2045.

Aulbach, S., Creaser, R.A., Pearson, N.J., Simonetti, S.S., Heaman, L.M., Griffin, W.L., Stachel, T., 2009. Sulfide and whole rock Re–Os systematics of eclogite and pyroxenite xenoliths from the Slave Craton, Canada. Earth Planet. Sci. Lett. 283, 48–58.

Aulbach, S., Sun, J., Tappe, S., Gerdes, A., 2019. Effects of multi-stage rifting and metasomatism on HSE-^{187}Os/^{188}Os systematics of the cratonic mantle beneath SW Greenland. Contrib. Mineral. Petrol. 174, 1–16.

Aulbach, S., Giuliani, A., Fiorentini, M.L., Baumgartner, R.J., Savard, D., Kamenetsky, V.S., Caruso, S., Danyushevky, L.V., Powell, W., Griffin, W.L., 2021. Siderophile and chalcophile elements in spinels, sulphides and native Ni in strongly metasomatised xenoliths from the Bultfontein kimberlite (South Africa). Lithos 380-381, 105880.

Blanks, D.E., Holwell, D.A., Fiorentini, M.L., Moroni, M., Giuliani, A., Tassara, S., González-Jiménez, J.M., Boyce, A.J., Ferrari, E., 2020. Fluxing of mantle carbon as a physical agent for metallogenic fertilization of the crust. Nat. Commun. 11, 1–11.

Büchl, A., Brügmann, G., Batanova, V.G., Münker, C., Hofmann, A.W., 2002. Melt percolation monitored by Os isotopes and HSE abundances: a case study from the mantle section of the Troodos Ophiolite. Earth Planet. Sci. Lett. 204, 385–402.

Chen, K., Tang, M., Lee, C.T.A., Wang, Z., Zou, Z., Hu, Z., Liu, Y., 2020. Sulfide-bearing cumulates in deep continental arcs: the missing copper reservoir. Earth Planet. Sci. Lett. 531, 115971.

Ciążela, J., Dick, H.J., Koepke, J., Pieterek, B., Muszynski, A., Botcharnikov, R., Kuhn, T., 2017. Thin crust and exposed mantle control sulfide differentiation in slow-spreading ridge magmas. Geology 45, 935–938.

Ciążela, J., Koepke, J., Dick, H.J., Botcharnikov, R., Muszynski, A., Lazarov, M., Schuth, S., Pieterek, B., Kuhn, T., 2018. Sulfide enrichment at an oceanic crust-mantle transition zone: Kane Megamullion (23°N, MAR). Geochim. Cosmochim. Acta 230, 155–189.
Ciążela, J., Weyer, S., Weyrauch, M., Horn, I., Dick, H.J.B., Pieterek, B., 2019. Ni-Fe isotope fractionation during cooling of sulfide liquid. Goldschmidt 2019 Abstracts.
Craddock, P.R., Warren, J.M., Dauphas, N., 2013. Abyssal peridotites reveal the near-chondritic Fe isotopic composition of the Earth. Earth Planet. Sci. Lett. 365, 63–76.
Craig, J.R., Kullerud, G., 1969. Phase relations in the Cu-Fe-Ni-S system and their application to magmatic ore deposits. Econ. Geol. Monogr. 4, 344–358.
Delpech, G., Lorand, J.P., Grégoire, M., Cottin, J.Y., O'Reilly, S.Y., 2012. In-situ geochemistry of sulfides in highly metasomatized mantle xenoliths from Kerguelen, southern Indian Ocean. Lithos 154, 296–314.
D'Errico, M.E., Coble, M.A., Warren, J.M., 2019. In situ measurements of lead and other trace elements in abyssal peridotite sulfides. Am. Mineral. 104, 190–206.
Ducea, M.N., Park, S.K., 2000. Enhanced mantle conductivity from sulfide minerals, southern Sierra Nevada, California. Geophys. Res. Lett. 27, 2405–2408.
Embey-Isztin, A., Downes, H., James, D.E., Upton, B.G.J., Dobosi, G., Ingram, G.A., Harmon, R.S., Scharbert, H.G., 1993. The petrogenesis of Pliocene alkaline volcanic rocks from the Pannonian Basin, Eastern Central Europe. J. Petrol. 34, 317–343.
Fellows, S.A., Canil, D., 2012. Experimental study of the partitioning of Cu during partial melting of Earth's mantle. Earth Planet. Sci. Lett. 337, 133–143.
Fodor, L., Csontos, L., Bada, G., Györfi, I., Benkovics, L., 1999. Tertiary tectonic evolution of the Pannonian Basin system and neighbouring orogens: a new synthesis of palaeostress data. Geol. Soc. Spec. Publ. 156, 295–334.
Garuti, G., Gorgoni, C., Sighinolfi, G.P., 1984. Sulfide mineralogy and chalcophile and siderophile element abundances in the Ivrea-Verbano mantle peridotites (Western Italian Alps). Earth Planet. Sci. Lett. 70, 69–87.
González-Jiménez, J.M., Villaseca, C., Griffin, W.L., O'Reilly, S.Y., Belousova, E., Ancochea, E., Pearson, N.J., 2014. Significance of ancient sulfide PGE and Re–Os signatures in the mantle beneath Calatrava, Central Spain. Contrib. Mineral. Petrol. 168, 1047.
González-Jiménez, J.M., Proenza, J.A., Pastor-Oliete, M., Saunders, E., Aiglsperger, T., Pujol-Solà, N., Melgarejo, J.C., Gervilla, F., Garcia-Casco, A., 2020. Precious metals in magmatic Fe-Ni-Cu sulfides from the Potosí chromitite deposit, eastern Cuba. Ore Geol. Rev. 118, 103339.
Grad, M., Tiira, T., ESC Working Group, 2009. The Moho depth map of the European Plate. Geophys. J. Int. 176, 279–292.
Griffin, W.L., Spetsius, Z.V., Pearson, N.J., O'Reilly, S.Y., 2002. In situ Re-Os analysis of sulfide inclusions in kimberlitic olivine: New constraints on depletion events in the Siberian lithospheric mantle. Geochem. Geophys. Geosyst. 3, 1–25.
Guillong, M., Meier, D.L., Allan, M.M., Heinrich, C.A., Yardley, B.W., 2008. Appendix A6: SILLS: a MATLAB-based program for the reduction of laser ablation ICP-MS data of homogeneous materials and inclusions. Mineral. Assoc. of Canada Short Course 40, 328–333.
Guo, J., Griffin, W.L., O'Reilly, S.Y., 1999. Geochemistry and origin of sulphide minerals in mantle xenoliths: Qilin, Southeastern China. J. Petrol. 40, 1125–1149.
Horn, I., von Blanckenburg, F., 2007. Investigation on elemental and isotopic fractionation during 196 nm femtosecond laser ablation multiple collector inductively coupled plasma mass spectrometry. Spectrochim. Acta 62, 410–422.
Horváth, F., 1993. Towards a mechanical model for the formation of the Pannonian basin. Tectonophysics 226, 333–357.
Horváth, F., Cloetingh, S.A.P.L., 1996. Stress-induced late-stage subsidence anomalies in the Pannonian basin. Tectonophysics 266, 287–300.
Horváth, F., Bada, G., Szafián, P., Tari, G., Ádám, A., Cloetingh, S., 2006. Formation and deformation of the Pannonian Basin: constraints from observational data. Geol. Soc. Mem. 32, 191–206.
Huang, F., Zhang, Z., Lundstrom, C.C., Zhi, X., 2011. Iron and magnesium isotopic compositions of peridotite xenoliths from Eastern China. Geochim. Cosmochim. Acta 75, 3318–3334.
Hurai, V., Danišík, M., Huraiová, M., Paquette, J.L., Ádám, A., 2013. Combined U/Pb and (U–Th)/he geochronometry of basalt maars in Western Carpathians: implications for age of intraplate volcanism and origin of zircon metasomatism. Contrib. Mineral. Petrol. 166, 1235–1251.
Jugo, P.J., Luth, R.W., Richards, J.P., 2005. An experimental study of the sulfur content in basaltic melts saturated with immiscible sulfide or sulfate liquids at 1300° C and 1 GPa. J. Petrol. 46, 783–798.
Kovács, I., Zajacz, Z., Cs, Szabó, 2004. Type-II xenoliths and related metasomatism from the Nógrád-Gömör Volcanic Field, Carpathian-Pannonian region (northern Hungary–southern Slovakia). Tectonophysics 393, 139–161.
Kullerud, G., Yund, R.A., Moh, G., 1969. Phase relations in Fe-Ni-S, Cu-Fe-S and Cu-Ni-S systems. Econ. Geol. 61, 804.
Liptai, N., Patkó, L., Kovács, I.J., Hidas, K., Zs, Pintér, Jeffries, T., Zajacz, Z., O'Reilly, S.Y., Griffin, W.L., Pearson, N.J., Cs, Szabó, 2017. Multiple metasomatism beneath the Nógrád–Gömör Volcanic Field (Northern Pannonian Basin) revealed by upper mantle peridotite xenoliths. J. Petrol. 58, 1107–1144.
Liptai, N., Hidas, K., Tommasi, A., Patkó, L., Kovács, I.J., Griffin, W.L., O'Reilly, S.Y., Pearson, N.J., Cs, Szabó, 2019. Lateral and vertical heterogeneity in the lithospheric mantle at the northern margin of the Pannonian Basin reconstructed from peridotite xenolith microstructures. J. Geophys. Res. - Sol. Ea. 124, 6315–6336.
Lorand, J.P., Grégoire, M., 2006. Petrogenesis of base metal sulphide assemblages of some peridotites from the Kaapvaal craton (South Africa). Contrib. Mineral. Petrol. 151, 521.
Lorand, J.P., Luguet, A., 2016. Chalcophile and siderophile elements in mantle rocks: Trace elements controlled by trace minerals. Rev. Mineral. Geochem. 81, 441–488.
Lorand, J.P., Alard, O., Luguet, A., Keays, R.R., 2003. Sulfur and selenium systematics of the subcontinental lithospheric mantle: inferences from the Massif Central xenolith suite (France). Geochim. Cosmochim. Acta 67, 4137–4151.
Lorand, J.P., Delpech, G., Grégoire, M., Moine, B., O'Reilly, S.Y., Cottin, J.Y., 2004. Platinum-group elements and the multistage metasomatic history of Kerguelen lithospheric mantle (South Indian Ocean). Chem. Geol. 208, 195–215.
Luguet, A., Reisberg, L., 2016. Highly siderophile element and ^{187}Os signatures in non-cratonic basalt-hosted peridotite xenoliths: unravelling the origin and evolution of the post-Archean lithospheric mantle. Rev. Mineral. Geochem. 81, 305–367.
Luguet, A., Shirey, S.B., Lorand, J.P., Horan, M.F., Carlson, R.W., 2007. Residual platinum-group minerals from highly depleted harzburgites of the Lherz massif (France) and their role in HSE fractionation of the mantle. Geochim. Cosmochim. Acta 71, 3082–3097.
Luguet, A., Pearson, D.G., Nowell, G.M., Dreher, S.T., Coggon, J.A., Spetsius, Z.V., Parman, S.W., 2008. Enriched Pt-Re-Os isotope systematics in plume lavas explained by metasomatic sulfides. Science 319, 453–456.
Mansur, E.T., Barnes, S.J., Duran, C.J., 2021. An overview of chalcophile element contents of pyrrhotite, pentlandite, chalcopyrite, and pyrite from magmatic Ni-Cu-PGE sulfide deposits. Mineral. Deposita 56, 179–204.
Mavrogenes, J.A., O'Neill, H.S.C., 1999. The relative effects of pressure, temperature and oxygen fugacity on the solubility of sulfide in mafic magmas. Geochim. Cosmochim. Acta 63, 1173–1180.
McCoy-West, A.J., Fitton, J.G., Pons, M.L., Inglis, E.C., Williams, H.M., 2018. The Fe and Zn isotope composition of deep mantle source regions: Insights from Baffin Island picrites. Geochim. Cosmochim. Acta 238, 542–562.
McDonough, W.F., Sun, S.S., 1995. The composition of the Earth. Chem. Geol. 120, 223–253.
Mungall, J.E., Su, S., 2005. Interfacial tension between magmatic sulfide and silicate liquids: Constraints on kinetics of sulfide liquation and sulfide migration through silicate rocks. Earth Planet. Sci. Lett. 234, 135–149.
Negishi, H., Arai, S., Yurimoto, H., Ito, S., Ishimaru, S., Tamura, A., Akizawa, N., 2013. Sulfide-rich dunite within a thick Moho transition zone of the northern Oman ophiolite: Implications for the origin of Cyprus-type sulfide deposits. Lithos 164, 22–35.
Oeser, M., Weyer, S., Horn, I., Schuth, S., 2014. High-precision fe and mg isotope ratios of silicate reference glasses determined in situ by femtosecond LA-MC-ICP-MS and by solution nebulisation MC-ICP-MS. Geostand. Geoanal. Res. 38, 311–328.
O'Neill, H.S.C., Mavrogenes, J.A., 2002. The sulfide capacity and the sulfur content at sulfide saturation of silicate melts at 1400 °C and 1 bar. J. Petrol. 43, 1049–1087.
Panayiotou, A., 1978. The mineralogy and chemistry of the podiform chromite deposits in the serpentinites of the Limassol Forest. Cyprus. *Miner. Deposita* 13, 259–274.
Patkó, L., Liptai, N., Aradi, L.E., Klébesz, R., Sendula, E., Bodnar, R.J., Kovács, I.J., Hidas, K., Cesare, B., Novák, A., Trásy, B., Cs, Szabó, 2020. Metasomatism-induced wehrlite formation in the upper mantle beneath the Nógrád-Gömör Volcanic Field (Northern Pannonian Basin): evidence from xenoliths. Geosci. Front. 11, 943–964.
Peslier, A.H., Francis, D., Ludden, J., 2002. The lithospheric mantle beneath continental margins: melting and melt–rock reaction in Canadian Cordillera xenoliths. J. Petrol. 43 (11), 2013–2047. https://doi.org/10.1093/petrology/43.11.2013.
Peters, B.J., Shahar, A., Carlson, R.W., Day, J.M., Mock, T.D., 2019. A sulfide perspective on iron isotope fractionation during ocean island basalt petrogenesis. Geochim. Cosmochim. Acta 245, 59–78.
Pieterek, B., Ciazela, J., Tribuzio, R., Muszyński, A., 2019. Towards understanding metal migration through subcontinental crust-mantle transition zones: first insights from the Ivrea-Verbano zone. Ofioliti 44, 29.
Poitrasson, F., Delpech, G., Grégoire, M., 2013. On the iron isotope heterogeneity of lithospheric mantle xenoliths: implications for mantle metasomatism, the origin of basalts and the iron isotope composition of the Earth. Contrib. Mineral. Petrol. 165, 1243–1258.
Polyakov, V.B., Soultanov, D.M., 2011. New data on equilibrium iron isotope fractionation among sulfides: Constraints on mechanisms of sulfide formation in hydrothermal and igneous systems. Geochim. Cosmochim. Acta 75, 1957–1974.
Pouchou, J.L., Pichoir, F., 1991. Quantitative analysis of homogeneous or stratified microvolumes applying the model "PAP". Electron Probe Quantitation. Springer US, pp. 31–75.
Reisberg, L., Zhi, X., Lorand, J.P., Wagner, C., Peng, Z., Zimmermann, C., 2005. Re–Os and S systematics of spinel peridotite xenoliths from east Central China: evidence for contrasting effects of melt percolation. Earth Planet. Sci. Lett. 239, 286–308.
Saunders, J.E., Pearson, N.J., O'Reilly, S.Y., Griffin, W.L., 2015. Sulfide metasomatism and the mobility of gold in the lithospheric mantle. Chem. Geol. 410, 149–161.
Saunders, J.E., Pearson, N.J., O'Reilly, S.Y., Griffin, W.L., 2016. Gold in the mantle: the role of pyroxenites. Lithos 244, 205–217.
Schuessler, J.A., Schoenberg, R., Sigmarsson, O., 2009. Iron and lithium isotope systematics of the Hekla volcano, Iceland - evidence for Fe isotope fractionation during magma differentiation. Chem. Geol. 258, 78–91.
Sillitoe, R.H., 2010. Porphyry copper systems. Econ. Geol. 105, 3–41.
Szabó, C.S., Bodnar, R.J., 1995. Chemistry and origin of mantle sulfides in spinel peridotite xenoliths from alkaline basaltic lavas, Nógraád-Gömör Volcanic Field, northern Hungary and southern Slovakia. Geochim. Cosmochim. Acta 59, 3917–3927.
Szabó, C.S., Taylor, L.A., 1994. Mantle petrology and geochemistry beneath the Nógrád-Gömör Volcanic Field, Carpathian-Pannonian Region. Int. Geol. Rev. 36, 328–358.
Szabó, C.S., Sz, Harangi, Csontos, L., 1992. Review of neogene and quaternary volcanism of the carpathian-pannonian region. Tectonophysics 208, 243–256.
Teng, F.Z., Dauphas, N., Helz, R.T., Gao, S., Huang, S., 2011. Diffusion-driven magnesium and iron isotope fractionation in Hawaiian olivine. Earth Planet. Sci. Lett. 308, 317–324.
Teng, F.Z., Dauphas, N., Huang, S., Marty, B., 2013. Iron isotopic systematics of oceanic basalts. Geochim. Cosmochim. Acta 107, 12–26.
Urey, H.C., 1947. The thermodynamic properties of isotopic substances. J. Chem. Soc. 562–581.

Wainwright, A.N., Luguet, A., Fonseca, R.O.C., Pearson, D.G., 2015. Investigating metasomatic effects on the ^{187}Os isotopic signature: a case study on micrometric base metal sulphides in metasomatised peridotite from the Letlhakane kimberlite (Botswana). Lithos 232, 35–48.
Wang, K.L., O'Reilly, S.Y., Griffin, W.L., Pearson, N.J., Zhang, M., 2009. Sulfides in mantle peridotites from Penghu Islands, Taiwan: melt percolation, PGE fractionation, and the lithospheric evolution of the South China block. Geochim. Cosmochim. Acta 73, 4531–4557.
Wang, Z., Lazarov, M., Steinmann, L.K., Becker, H., Zou, Z., Geng, X., 2018. The distribution of lead and thallium in mantle rocks: Insights from the Balmuccia peridotite massif (Italian Alps). Am. Mineral. 103, 1185–1199.
Westner, K.J., Beier, C., Klemd, R., Osbahr, I., Brooks, N., 2019. In Situ Chalcophile and Siderophile Element Behavior in Sulfides from Moroccan Middle Atlas Spinel Peridotite Xenoliths during Metasomatism and Weathering. Minerals 9, 276.
Weyer, S., Ionov, D.A., 2007. Partial melting and melt percolation in the mantle: the message from Fe isotopes. Earth Planet. Sci. Lett. 259, 119–133.
Zajacz, Z., Cs, Szabó, 2003. Origin of sulfide inclusions in cumulate xenoliths from Nógrád–Gömör Volcanic Field, Pannonian Basin (North Hungary/South Slovakia). Chem. Geol. 194, 105–117.
Zajacz, Z., Kovács, I., Cs, Szabó, Halter, W., Pettke, T., 2007. Evolution of mafic alkaline melts crystallized in the uppermost lithospheric mantle: a melt inclusion study of olivine-clinopyroxenite xenoliths, northern Hungary. J. Petrol. 48, 853–883.
Zhang, Z., Hirschmann, M.M., 2016. Experimental constraints on mantle sulfide melting up to 8 GPa. Am. Mineral. 101, 181–192.
Zhang, L., Sun, W.D., Zhang, Z.F., An, Y., Liu, F., 2020. Iron isotope behavior during melt-peridotite interaction in supra-subduction zone ophiolite from Northern Tibet. J. Geophys. Res. - Sol. Ea 125 e2019JB018823.
Zhao, X., Zhang, H., Zhu, X., Tang, S., Tang, Y., 2010. Iron isotope variations in spinel peridotite xenoliths from North China Craton: implications for mantle metasomatism. Contrib. Mineral. Petrol. 160, 1–14.
Zhao, X., Zhang, H., Zhu, X., Tang, S., Yan, B., 2012. Iron isotope evidence for multistage melt–peridotite interactions in the lithospheric mantle of eastern China. Chem. Geol. 292, 127–139.